J Math Chem (2010) 47:590–625
DOI 10.1007/s10910-009-9587-4

ORIGINAL PAPER

Infrared transmission equations in a five media system: gas and liquid

Jean-Joseph Max · Camille Chapados

Received: 28 April 2009 / Accepted: 10 August 2009 / Published online: 9 September 2009

Abstract Equations are proposed for transmission cells in the presence of multiple reflections and absorption which generate unwanted fringes. These influence adversely band intensity measurements. The infrared (IR) spectra generated with these equations are compared successfully with experimental spectra obtained with BaF_2, ZnSe, and Si windows in parallel mount formation having μm range air gaps. Equations are extended for integration of a variable path length such as in wedge shaped cells that are used to mitigate fringe formations but generate other odd problems such as path length determination. These equations allow the evaluation of the transmission obtained from boxcar cells whose parallelism is a little offset. This phenomenon modifies the fringe intensities. The proposed equations were used to calculate the IR spectra of pure liquid D_2O between BaF_2 and ZnSe windows with path lengths of around 25 μm and compared with experimental spectra. Since the fit was very good it indicates that the proposed equations give better optical properties of pure liquids than that presently available. This is important for liquid used as standards and in particular water used here as reference.

Keywords Infrared · Transmission equations · Five media systems · Gas · Liquid · Multiple reflections · Fringes

J.-J. Max · C. Chapados (✉)
Département de chimie–biologie, Université du Québec à Trois-Rivières,
C.P. 500, Trois-Rivieres, QC G9A 5H7, Canada
e-mail: Camille.Chapados@uqtr.ca

Present Address:
J.-J. Max
ITF Labs, 400 Montpellier, Montreal, QC H4N 2G7, Canada
e-mail: jjmax@itflabs.com

1 Introduction

We recently published detailed analysis of liquid water infrared (IR) spectra. First with H_2O–D_2O mixtures and, second, with light and heavy water as a function of temperature [1,2]. The spectra in these were obtained by attenuated total reflection (ATR) that gave highly reproducible spectra so that factor analysis (FA) was fruitfully used. Since this analytical method is quantitative it permitted us to obtain fundamental information on liquid water. However, this information is not complete because the far IR (FIR) region is lacking since ATR needs crystals. Since these are not transparent in the FIR we cannot use that technique to obtain the spectra in that region. The water studies and previous ones in aqueous solutions indicate that for a comprehensive understanding of liquid water systems one needs the complete IR spectra from 0 to at least 4,000 cm^{-1} [1–11]. This spectral region covers the absorption of the covalent and intermolecular bonds. Since the FIR region is not accessible by ATR we rely on transmission measurements that are, however, perturbed by absorption and reflection at the window's interface giving the spectra a strong sinusoidal pattern.

Papers reporting on the transmission technique generally ignore the multiple reflection problems or use over simplifying assumptions that mitigate the problem. Some approximate methods were developed that decrease and sometimes eliminated the unwanted interference fringes [12–23]. Several years ago, Crawford et al. evaluated this phenomenon and concluded that investigators interested in liquid IR intensity measurements should avoid transmission measurements and, instead, use the ATR sampling method [24]. Although we agree with this recommendation, the transmission technique is sometimes unavoidable since the ATR technique does not give the spectra in the FIR. Only a few quantitative methods were developed for evaluating accurately the transmission spectrum of a system with multiple reflections [18,23,25–27]. Kucirkova and Navratil were one of the few that proposed a solution for the IR measurements of liquids. To deal with the lack of parallelism of the windows they integrated the transmission over the cell thickness [18]. However, they did not give the integration in an analytical form which renders this method inapplicable.

The concatenation of the mid IR (MIR) spectra coming from ATR measurements and FIR spectra coming from transmission measurements is not a simple matter of joining the spectra coming from both regions since the optical characteristics of the two methods are different. To obtain irreducible data between them we have to transform the experimental spectra, which are instrument and sampling method dependent, into the sample optical properties that only depend on the sample. This is done with the Kramers–Kronig relation, which links both real and imaginary parts of the refractive index but requires the spectra from null frequency up to "infinite" frequency [8–11,28]. Spectra obtained by transmission measurements can fill the gap. However, the only suitable window material for FIR is silicon (Si) which has a high refractive index that produces multiple reflections. Moreover, close to strong bands, the material refractive index varies considerably modifying the sinusoidal pattern. A strong band eliminates completely internal reflection in the band range. These perturbations make accurate IR intensity measurements difficult. Liquid water is one of the worst cases. In the 4,000–0 cm^{-1} region the real part of the water refractive index varies widely: from 1.1 to 1.5 in the OH stretch region (3,600–3,200 cm^{-1}) and from 1.1 to 8.0 in the

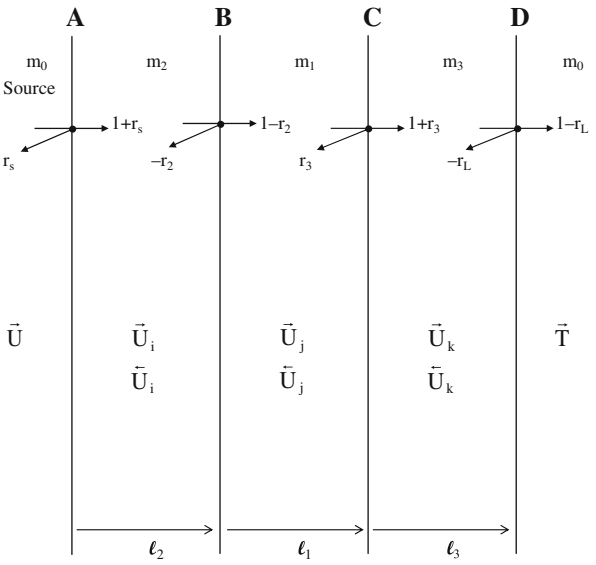

Fig. 1 Transmission cell and travelling waves. *A*, *B*, *C*, and *D* are the separating interfaces of optical media m_0, m_2, m_1, m_3, and m_0, respectively. The reflection coefficients are r_s, r_2, r_3 and r_L, respectively. The electric fields are: $\overrightarrow{U}$ in incident medium m_0, $\overrightarrow{U}_i$ and $\overleftarrow{U}_i$ in medium m_2, $\overrightarrow{U}_j$ and $\overleftarrow{U}_j$ in medium m_1, $\overrightarrow{U}_k$ and $\overleftarrow{U}_k$ in medium m_3 and $\overrightarrow{T}$ in output medium m_0. The origin of each traveling waves is on the left side of the corresponding medium except for the incident waves $\overrightarrow{U}$ and $\overleftarrow{U}$ for which the origin is at interface A. ℓ_i is pathlength i

$900–0\,cm^{-1}$ region. No IR window material can match these variations. This in turn makes it impossible the elimination of the multiple reflections in the IR cells. These difficulties are responsible for the variations in the water optical properties reported that are often outside the stated accuracy [11,29–31].

The purpose of the present work is to provide the analytical equations for evaluating the transmission spectrum of a sample in between two windows of known optical properties. We will use these to characterize first the situation of an air sample confined between pairs of windows of different refractive indices to verify the exactness of the transmission equations. Thereafter, we will tackle the situation of the IR transmitted in a liquid water sample situated between two windows. In these the multiple reflections and absorption modify the intensity of the band giving false intensity values. This is the phenomenon that prompted us to evaluate thoroughly the reflection–absorption phenomena in the IR because some pieces did not fit properly in the puzzle.

2 Theoretical

A light signal passing at normal incidence through a sample encounters four interfaces that separate five regions occupied by four different media. The input and output media are the same. They are considered to be infinite, that is: no reflections are coming back from their furthest extremity. Therefore, the problem is to evaluate the transmission spectrum of a sample (medium m_1) of thickness ℓ_1 embedded between two windows of media m_2 and m_3 of lengths ℓ_2 and ℓ_3, respectively. These constitute the measuring cell which we place in air (medium m_0). Figure 1 gives a schematic description of the travelling waves and the mathematical notations used in the equations.

2.1 Definitions

The four separating interfaces between successive optical media m_0, m_2, m_1, m_3, and m_0 are labeled A, B, C, and D, respectively (Fig. 1). For symmetry considerations, the reflection coefficients are denoted r_s, r_2, r_3 and r_L from medium m_0 to m_2, m_1 to m_2, m_1 to m_3 and m_0 to m_3, respectively.

2.2 Calculation of the transmission in a standing wave regime

Considering the light beam in a standing wave regime, the electromagnetic waves are indicated by the following electric fields [32]: $\overrightarrow{U}$ in incident medium m_0, $\overrightarrow{U}_i$ and $\overleftarrow{U}_i$ in medium m_2, $\overrightarrow{U}_j$ and $\overleftarrow{U}_j$ in medium m_1, $\overrightarrow{U}_k$ and $\overleftarrow{U}_k$ in medium m_3 and finally $\overrightarrow{T}$ in output medium m_0. Electric fields $\overleftarrow{U}$ in incident medium m_0 and $\overleftarrow{T}$ in output medium m_0 are not displayed in Fig. 1 due to the infinite nature of both section of medium m_0, $\overleftarrow{T}$ does not exists and $\overleftarrow{U}$ will not produce any component to be included into $\overrightarrow{U}$. The time, location and frequency dependence of the electrical vectors were removed where they were implicit. The origin of each traveling waves is on the left side of the corresponding medium except for the incident waves $\overrightarrow{U}$ and $\overleftarrow{U}$ for which the origin is at interface A.

2.2.1 General case: calculation of the complex transmission of a three layer system

The following calculations are made by assuming a stationary state. The reflection coefficients are complex values. At interface D the transmission relation is given by [32]:

$$\overrightarrow{T} = \overrightarrow{U}_k(\ell_3) \times (1 - r_L) = E_3 \overrightarrow{U}_k(0) \times (1 - r_L) \tag{1}$$

where E_3 is the propagation term of wave $\overrightarrow{U}_k$ from interface C to D (length ℓ_3). Similarly, at interface C, we have:

$$\overrightarrow{U}_k(0) = E_1 \overrightarrow{U}_j(0) \times (1 + r_3) + E_3^2 \overrightarrow{U}_k(0) \times r_3 r_L \tag{2}$$

where E_1 is the propagation term of wave $\overrightarrow{U}_j$ from interface B to C (length ℓ_1). Equation (2) gives:

$$\overrightarrow{U}_k(0) = \frac{(1 + r_3)\ E_1}{1 - r_3 r_L\ E_3^2} \overrightarrow{U}_j(0) \tag{3}$$

Similarly, after combining the results at interface B and A one obtains the cell transmission:

$$\overrightarrow{\mathrm{T}} = \frac{(1-\mathrm{r_L})(1+\mathrm{r_3})(1-\mathrm{r_2})(1+\mathrm{r_s})\,\mathrm{E_1E_2E_3}}{\left(1-\mathrm{r_3r_L}\mathrm{E_3^2}\right)\left(1-\mathrm{r_2r_s}\mathrm{E_2^2}\right)-\mathrm{E_1^2}\left(\mathrm{r_2}-\mathrm{r_s}\mathrm{E_2^2}\right)\left(\mathrm{r_3}-\mathrm{r_L}\mathrm{E_3^2}\right)}\overrightarrow{\mathrm{U}}(0) \tag{4}$$

2.2.2 Windows of same material

In spectroscopy, the cell windows are made of the same material. Because of this $\mathrm{r_2} = \mathrm{r_3}$ and $\mathrm{r_s} = \mathrm{r_L}$ which gives for Eq. 4:

$$\overrightarrow{\mathrm{T}} = \frac{\left(1-\mathrm{r_s^2}\right)\left(1-\mathrm{r_2^2}\right)\,\mathrm{E_1E_2E_3}}{\left(1-\mathrm{r_2r_s}\mathrm{E_3^2}\right)\left(1-\mathrm{r_2r_s}\mathrm{E_2^2}\right)-\mathrm{E_1^2}\left(\mathrm{r_2}-\mathrm{r_s}\mathrm{E_2^2}\right)\left(\mathrm{r_2}-\mathrm{r_s}\mathrm{E_3^2}\right)}\overrightarrow{\mathrm{U}}(0) \tag{5}$$

with $\mathrm{r_s} = \frac{n_2-1}{n_2+1}$ and $\mathrm{r_2} = \frac{n_2-n_1}{n_2+n_1}$.

The propagation term in medium x is [25]:

$$\begin{cases} \mathrm{I_x} = \|\mathrm{E_x}\|^2 = \mathrm{e}^{-\frac{4\pi\nu}{\mathrm{c}}k_x\ell_x} \\ \alpha_\mathrm{x} = \frac{4\pi\nu}{\mathrm{c}}k_x\ell_x \\ \mathrm{E_x} = \mathrm{e}^{-\mathrm{j}\mathrm{K_x}\ell_x} \times \mathrm{e}^{-\frac{\alpha_\mathrm{x}}{2}} = \mathrm{e}^{-j\frac{2\pi\nu}{\mathrm{c}}n_x\ell_x} \times \mathrm{e}^{-\frac{2\pi\nu}{\mathrm{c}}k_x\ell_x} \end{cases} \tag{6}$$

where $\mathrm{K_x}\ell_x$ is the scalar product of the propagation and displacement vectors, α_x is the loss term (absorption); ν, the wave frequency; n_x and k_x, the real and imaginary parts of the refractive index; respectively, and c the speed of light in vacuum. Equation 5 indicates that the output wave $\overrightarrow{\mathrm{T}}$ is a complex expression whose amplitude (norm) is measured as a function of frequency. Since $\overrightarrow{\mathrm{T}}$ and $\overrightarrow{\mathrm{U}}(0)$ are collinear, the overall transmission T of the cell can be written as complex number ratio: $(\eta + \mathrm{j}\xi)/(\chi + \mathrm{j}\mu)$. Hence:

$$\mathrm{T} = \frac{\left\|\overrightarrow{\mathrm{T}}\right\|^2}{\left\|\overrightarrow{\mathrm{U}}(0)\right\|^2} = \frac{\eta^2+\xi^2}{\chi^2+\mu^2} \tag{7}$$

To simplify the equations we introduce the propagation delay term, T_x associated to the angular frequency $\omega = 2\pi\nu$:

$$n_x\ell_x 2\pi\nu/\mathrm{c} = \omega\mathrm{T_x} \tag{8}$$

Equation 5 becomes:

$$\overrightarrow{\mathrm{T}} = \frac{\left(1-\mathrm{r_s^2}\right)\left(1-\mathrm{r_2^2}\right)\,\mathrm{e}^{-\frac{\alpha_1+\alpha_2+\alpha_3}{2}}\,\mathrm{e}^{-\mathrm{j}\omega(\mathrm{T_1}+\mathrm{T_2}+\mathrm{T_3})}}{\left(1-\mathrm{r_2r_s}\mathrm{e}^{-\alpha_2}\,\mathrm{e}^{-2\mathrm{j}\omega\mathrm{T_2}}\right)\left(1-\mathrm{r_2r_s}\mathrm{e}^{-\alpha_3}\,\mathrm{e}^{-2\mathrm{j}\omega\mathrm{T_3}}\right)-\mathrm{e}^{-\alpha_1}\,\mathrm{e}^{-2\mathrm{j}\omega\mathrm{T_1}}\left(\mathrm{r_2}-\mathrm{r_s}\mathrm{e}^{-\alpha_2}\mathrm{e}^{-2\mathrm{j}\omega\mathrm{T_2}}\right)\left(\mathrm{r_2}-\mathrm{r_s}\mathrm{e}^{-\alpha_3}\mathrm{e}^{-2\mathrm{j}\omega\mathrm{T_3}}\right)} \times \overrightarrow{\mathrm{U}}(0) \tag{9}$$

After reorganization, one obtains for Eqs. 9 and 7:

$$T = \frac{\left(1 - r_s^2\right)^2 \left(1 - r_2^2\right)^2 \ e^{-(\alpha_1+\alpha_2+\alpha_3)}}{Re^2\,(D) + Im^2\,(D)} \tag{10}$$

where D is the complex denominator of the rightmost term in Eq. 9. The Eq. 10 numerator contains the sample attenuation (absorption) ($e^{-\alpha_1/2}$ term) and the denominator contains the resonant (or oscillating) term coming from the multiple reflections.

Developing the complex exponential terms in Eq. 9 gives:

$$D = \begin{cases} \left[1 - r_2 r_s e^{-\alpha_2} \cos\left(2\omega T_2\right) + j r_2 r_s e^{-\alpha_2} \sin\left(2\omega T_2\right)\right] \times \left[1 - r_2 r_s e^{-\alpha_3} \cos\left(2\omega T_3\right) + j r_2 r_s e^{-\alpha_3} \sin\left(2\omega T_3\right)\right] \\ - \left[e^{-\alpha_1} \cos\left(2\omega T_1\right) - j e^{-\alpha_1} \sin\left(2\omega T_1\right)\right] \\ \times \left[r_2 - r_s e^{-\alpha_2} \cos\left(2\omega T_2\right) + j r_s e^{-\alpha_2} \sin\left(2\omega T_2\right)\right] \times \left[r_2 - r_s e^{-\alpha_3} \cos\left(2\omega T_3\right) + j r_s e^{-\alpha_3} \sin\left(2\omega T_3\right)\right] \end{cases} \tag{11}$$

Separating the real [Re(D)] and imaginary [Im(D)] parts in D gives:

$$Re\,(D) = \begin{cases} 1 - r_2^2 e^{-\alpha_1} \cos\left(2\omega T_1\right) - r_2 r_s e^{-\alpha_2} \cos\left(2\omega T_2\right) - r_2 r_s e^{-\alpha_3} \cos\left(2\omega T_3\right) \\ + r_2 r_s e^{-(\alpha_1+\alpha_2)} \cos\left(2\omega\left(T_1 + T_2\right)\right) + r_2 r_s e^{-(\alpha_1+\alpha_3)} \\ \times \cos\left(2\omega\left(T_1 + T_3\right)\right) + r_2^2 r_s^2 e^{-(\alpha_2+\alpha_3)} \cos\left(2\omega\left(T_2 + T_3\right)\right) \\ - r_s^2 e^{-(\alpha_1+\alpha_2+\alpha_3)} \cos\left(2\omega\left(T_1 + T_2 + T_3\right)\right) \end{cases} \tag{12}$$

$$Im\,(D) = \begin{cases} - r_2^2 e^{-\alpha_1} \sin\left(2\omega T_1\right) + r_2 r_s \left[e^{-\alpha_2} \sin\left(2\omega T_2\right) + e^{-\alpha_3} \sin\left(2\omega T_3\right)\right] \\ - r_2 r_s e^{-(\alpha_1+\alpha_2)} \sin\left(2\omega\left(T_1 + T_2\right)\right) - r_2 r_s e^{-(\alpha_1+\alpha_3)} \\ \times \sin\left(2\omega\left(T_1 + T_3\right)\right) - r_2^2 r_s^2 e^{-(\alpha_2+\alpha_3)} \sin\left(2\omega\left(T_2 + T_3\right)\right) \\ + r_s^2 e^{-(\alpha_1+\alpha_2+\alpha_3)} \sin\left(2\omega\left(T_1 + T_2 + T_3\right)\right) \end{cases} \tag{13}$$

Due to the 2 ωT_i terms, Re(D) and Im(D) oscillate with ν. In ordinary conditions, the window thickness is far larger than that of the sample. Therefore, the terms that vary the most rapidly in D are those with T_2 or T_3. Assuming $T_1 << T_2$, and $T_1 << T_3$, the fastest variation of Re(D) and Im(D) will occur within the condition: $2\omega T_i = 2m\pi\,(i = 2, 3)$, when m increases by one unit. That is:

$$n_i \ell_i 2\pi\nu/c = \omega T_i = m\pi \tag{14}$$

where c is the speed of light (in m/s). ν/c replaced by $100\tilde{\nu}$ gives the values in wavenumber (cm^{-1}). The interval ($\Delta\tilde{\nu}$) that produces an almost complete oscillation of Re(D) and Im(D) is:

$$\Delta\tilde{\nu} = 1/200 n_i \ell_i \tag{15}$$

For thick samples, the oscillations are very weak and consequently difficult to observe. However, they are unavoidable and one must be aware of their existence and try to minimize them.

2.2.3 Removing the window fast oscillations

The oscillations features generated by thick windows can be eliminated in numerical calculations. This is done by separating the slow from the fast oscillating terms. Therefore, from Eqs. (12) and (13) one gets:

$$\mathrm{Re\,(D)} = \begin{cases} 1 - r_2^2 e^{-\alpha_1}\cos(2\omega T_1) + \cos(2\omega T_1)[r_2 r_s e^{-(\alpha_1+\alpha_3)}\cos(2\omega T_3) \\ \quad + r_2 r_s e^{-(\alpha_1+\alpha_2)}\cos(2\omega T_2) - r_s^2 e^{-(\alpha_1+\alpha_2+\alpha_3)}\cos(2\omega\{T_2+T_3\})] \\ \quad - \sin(2\omega T_1)[r_2 r_s e^{-(\alpha_1+\alpha_3)}\sin(2\omega T_3) + r_2 r_s e^{-(\alpha_1+\alpha_2)} \\ \quad \times \sin(2\omega T_2) - r_s^2 e^{-(\alpha_1+\alpha_2+\alpha_3)}\sin(2\omega\{T_2+T_3\})] - r_2 r_s e^{-\alpha_2} \\ \quad \times\cos(2\omega T_2) - r_2 r_s e^{-\alpha_3}\cos(2\omega T_3) + r_2^2 r_s^2 e^{-(\alpha_2+\alpha_3)}\cos(2\omega(T_2+T_3)) \end{cases} \tag{16}$$

$$\mathrm{Im(D)} = \begin{cases} -r_2^2 e^{-\alpha_1}\sin(2\omega T_1) + \sin(2\omega T_1)[-r_2 r_s e^{-(\alpha_1+\alpha_3)}\cos(2\omega T_3) \\ \quad - r_2 r_s e^{-(\alpha_1+\alpha_2)}\cos(2\omega T_2) + r_s^2 e^{-(\alpha_1+\alpha_2+\alpha_3)}\cos(2\omega\{T_2+T_3\})] \\ \quad + \cos(2\omega T_1)[-r_2 r_s e^{-(\alpha_1+\alpha_3)}\sin(2\omega T_3) - r_2 r_s e^{-(\alpha_1+\alpha_2)} \\ \quad \times\sin(2\omega T_2) + r_s^2 e^{-(\alpha_1+\alpha_2+\alpha_3)}\sin(2\omega\{T_2+T_3\})] + r_2 r_s[e^{-\alpha_2} \\ \quad \times\sin(2\omega T_2) + e^{-\alpha_3}\sin(2\omega T_3)] - r_2^2 r_s^2 e^{-(\alpha_2+\alpha_3)}\sin(2\omega(T_2+T_3)) \end{cases} \tag{17}$$

In these the first lines contain the slow varying terms (with frequency). The three other lines are quick varying terms that contain the window large periods T_2 and T_3.

Since the numerator in Eq. (10) contains no oscillating terms it is sufficient to eliminate the interference fringes to integrate the denominator and consider constant the sample properties (valid in a small frequency interval). Integration of Re(D) and Im(D) over a complete period for T_2 and T_3 (where a complete period is $T_2 + T_3$) will eliminate all terms in $\cos 2\omega T_i$ and $\sin 2\omega T_i$ where $T_i = T_2$, T_3, or $T_2 + T_3$, so that:

$$\begin{cases} \mathrm{Re\,(D)} = 1 - r_2^2 e^{-\alpha_1}\cos(2\omega T_1) \\ \mathrm{Im\,(D)} = -r_2^2 e^{-\alpha_1}\sin(2\omega T_1) \end{cases} \tag{18}$$

With this, Eq. (10) becomes:

$$\begin{aligned} T &= \frac{\left(1-r_s^2\right)^2\left(1-r_2^2\right)^2\ e^{-\frac{\alpha_1+\alpha_2+\alpha_3}{2}}}{\left[1-r_2^2 e^{-\alpha_1}\cos(2\,\omega\,T_1)\right]^2 + \left[-r_2^2 e^{-\alpha_1}\sin(2\,\omega\,T_1)\right]^2} \\ &= \frac{\left(1-r_s^2\right)^2\left(1-r_2^2\right)^2\ e^{-\frac{\alpha_1+\alpha_2+\alpha_3}{2}}}{1-2r_2^2 e^{-\alpha_1}\cos(2\,\omega\,T_1) + r_2^4 e^{-2\alpha_1}} \end{aligned} \tag{19}$$

Equation (19) looks like Zelsmann's Eq. (10a) [22] with, however, some differences. In his equation, an erroneous factor of four is present in the denominator; the reflections at air/window interfaces are not considered and the term $|r_2^2|$ is used instead of the complex value r_2^2. However, this relation is correct for a single reflection but not for multiple ones which is the case in real situations. For these reasons Eq. (19) is favored over Zelsmann's one.

2.3 Background measurement: the case of an air sample

The transmission spectrum of the empty cell is required before that of a sample to correct for the window's absorption. The calculations for an air sample are obtained by making $r_2 = r_s = r = \frac{n_2-1}{n_2+1}$ and $\alpha_1 = 0$. This gives for Eq. (9):

$$\overrightarrow{\mathrm{T}} = \frac{\left(1-\mathrm{r}^2\right)^2 \, \mathrm{e}^{-\frac{\alpha_2+\alpha_3}{2}} \, \mathrm{e}^{-\mathrm{j}\omega(\mathrm{T}_1+\mathrm{T}_2+\mathrm{T}_3)}}{\left(1-\mathrm{r}^2\mathrm{e}^{-\alpha_2}\,\mathrm{e}^{-2\mathrm{j}\omega\mathrm{T}_2}\right)\left(1-\mathrm{r}^2\mathrm{e}^{-\alpha_3}\,\mathrm{e}^{-2\mathrm{j}\omega\mathrm{T}_3}\right)-\mathrm{r}^2\mathrm{e}^{-2\mathrm{j}\omega\mathrm{T}_1}\left(1-\mathrm{e}^{-\alpha_2}\,\mathrm{e}^{-2\mathrm{j}\omega\mathrm{T}_2}\right)\left(1-\mathrm{e}^{-\alpha_3}\,\mathrm{e}^{-2\mathrm{j}\omega\mathrm{T}_3}\right)} \times \overrightarrow{\mathrm{U}}(0) \tag{20}$$

After transformation, the denominator becomes:

$$\begin{aligned}\mathrm{D} = &\left[1-\mathrm{r}^2\mathrm{e}^{-\alpha_2}\cos(2\omega\mathrm{T}_2)+\mathrm{j}\mathrm{r}^2\mathrm{e}^{-\alpha_2}\sin(2\omega\mathrm{T}_2)\right]\\ &\times\left[1-\mathrm{r}^2\mathrm{e}^{-\alpha_3}\cos(2\omega\mathrm{T}_3)+\mathrm{j}\mathrm{r}^2\mathrm{e}^{-\alpha_3}\sin(2\omega\mathrm{T}_3)\right]\\ &-\mathrm{r}^2\left[\cos(2\omega\mathrm{T}_1)-\mathrm{j}\sin(2\omega\mathrm{T}_1)\right]\\ &\times\left[1-\mathrm{e}^{-\alpha_2}\cos(2\omega\mathrm{T}_2)+\mathrm{j}\mathrm{e}^{-\alpha_2}\sin(2\omega\mathrm{T}_2)\right]\\ &\times\left[1-\mathrm{e}^{-\alpha_3}\cos(2\omega\mathrm{T}_3)+\mathrm{j}\mathrm{e}^{-\alpha_3}\sin(2\omega\mathrm{T}_3)\right]\end{aligned} \tag{21}$$

Separating the real and imaginary parts in D gives:

$$\begin{cases}\begin{aligned}\mathrm{Re}(\mathrm{D}) = &1-\mathrm{r}^2\cos(2\omega\mathrm{T}_1)-\mathrm{r}^2\mathrm{e}^{-\alpha_2}\cos(2\omega\mathrm{T}_2)+\mathrm{r}^2\mathrm{e}^{-\alpha_2}\cos(2\omega(\mathrm{T}_1+\mathrm{T}_2))\\ &-\mathrm{r}^2\mathrm{e}^{-\alpha_3}\cos(2\omega\mathrm{T}_3)+\mathrm{r}^2\mathrm{e}^{-\alpha_3}\cos(2\omega(\mathrm{T}_1+\mathrm{T}_3))+\mathrm{r}^4\mathrm{e}^{-(\alpha_2+\alpha_3)}\\ &\times\cos(2\omega(\mathrm{T}_2+\mathrm{T}_3))-\mathrm{r}^2\mathrm{e}^{-(\alpha_2+\alpha_3)}\cos(2\omega(\mathrm{T}_1+\mathrm{T}_2+\mathrm{T}_3))\\ \mathrm{Im}(\mathrm{D}) = &-\mathrm{r}^2\mathrm{e}^{-\alpha_1}\sin(2\omega\mathrm{T}_1)-\mathrm{r}^2\left[\mathrm{e}^{-\alpha_2}\sin(2\omega\mathrm{T}_2)+\mathrm{e}^{-\alpha_3}\sin(2\omega\mathrm{T}_3)\right]\\ &+\mathrm{r}^4\mathrm{e}^{-(\alpha_2+\alpha_3)}\sin(2\omega(\mathrm{T}_2+\mathrm{T}_3))+\mathrm{r}^2\mathrm{e}^{-(\alpha_1+\alpha_3)}\sin(2\omega(\mathrm{T}_1+\mathrm{T}_3))\\ &+\mathrm{r}^2\mathrm{e}^{-(\alpha_1+\alpha_2)}\sin(2\omega(\mathrm{T}_1+\mathrm{T}_2))\\ &+\mathrm{r}^2\mathrm{e}^{-(\alpha_1+\alpha_2+\alpha_3)}\sin(2\omega(\mathrm{T}_1+\mathrm{T}_2+\mathrm{T}_3))\end{aligned}\end{cases} \tag{22}$$

It is verified that Eqs. (12), (13) and (22) give identical results for an air sample. Eq. (22) can be further reorganized and simplified into:

$$\begin{aligned}\mathrm{Re}(\mathrm{D}) = &1-\mathrm{r}^2\cos(2\omega\mathrm{T}_1)-2\mathrm{r}^2\mathrm{e}^{-\alpha_2}\sin(\omega(\mathrm{T}_1+2\mathrm{T}_2))\sin(\omega\mathrm{T}_1)-2\mathrm{r}^2\mathrm{e}^{-\alpha_3}\\ &\times\sin(\omega(\mathrm{T}_1+2\mathrm{T}_3))\sin(\omega\mathrm{T}_1)+\mathrm{r}^4\mathrm{e}^{-(\alpha_2+\alpha_3)}\cos(2\omega(\mathrm{T}_2+\mathrm{T}_3))\\ &-\mathrm{r}^2\mathrm{e}^{-(\alpha_2+\alpha_3)}\cos(2\omega(\mathrm{T}_1+\mathrm{T}_2+\mathrm{T}_3))\end{aligned} \tag{23}$$

$$\begin{aligned}\mathrm{Re}(\mathrm{D}) = &1-\mathrm{r}^2\cos(2\omega\mathrm{T}_1)-2\mathrm{r}^2\sin(\omega\mathrm{T}_1)\left\{\mathrm{e}^{-\alpha_2}\sin(\omega(\mathrm{T}_1+2\mathrm{T}_2))\right.\\ &\left.+\mathrm{e}^{-\alpha_3}\sin(\omega(\mathrm{T}_1+2\mathrm{T}_3))-\mathrm{e}^{-(\alpha_2+\alpha_3)}\sin(\omega(\mathrm{T}_1+2\mathrm{T}_2+2\mathrm{T}_3))\right\}\\ &-\mathrm{r}^2\left(1-\mathrm{r}^2\right)\mathrm{e}^{-(\alpha_2+\alpha_3)}\cos(2\omega(\mathrm{T}_2+\mathrm{T}_3))\end{aligned} \tag{24}$$

2.4 Absorbing sample: complex refractive index

2.4.1 General case: two identical windows

An absorbing sample will display a complex refractive index ($n_1^* = n_1 + \mathrm{j}k_1$) which will produce a complex reflection coefficient, r_2^*:

$$\begin{cases} \mathrm{r}_2^* = \dfrac{n_2 - n_1^*}{n_2 + n_1^*} = \dfrac{n_2 - (n_1 + \mathrm{j}k_1)}{n_2 + (n_1 + \mathrm{j}k_1)} = \mathrm{r}_{2R} + \mathrm{j}\mathrm{r}_{2I} \\ \mathrm{r}_{2R} = \dfrac{n_2^2 - n_1^2 - k_1^2}{(n_2 + n_1)^2 + k_1^2} \\ \mathrm{r}_{2I} = -2\dfrac{n_2 k_1}{(n_2 + n_1)^2 + k_1^2} \end{cases} \tag{25}$$

This introduced into Eq. (9) modifies Eq. (10) into:

$$\mathrm{T} = \frac{\left(1 - \mathrm{r}_\mathrm{s}^2\right)^2 \left\| 1 - \mathrm{r}_2^{*2} \right\|^2 \mathrm{e}^{-(\alpha_1 + \alpha_2 + \alpha_3)}}{\mathrm{Re}^2\,(\mathrm{D}) + \mathrm{Im}^2\,(\mathrm{D})} \tag{26}$$

Since the amplitude of the product of two complex numbers is equal to their product amplitudes, the numerator amplitude will only change with the amplitude term $(1 - \mathrm{r}_2^{*2})$. The denominator (D) amplitude requires more attention. Equation (11) becomes:

$$\mathrm{D} = \begin{cases} \left(1 - \left[\mathrm{r}_{2R} + \mathrm{j}\mathrm{r}_{2I}\right]\mathrm{r}_\mathrm{s}\mathrm{e}^{-\alpha_2}\left[\cos(2\omega\mathrm{T}_2) - \mathrm{j}\sin(2\omega\mathrm{T}_2)\right]\right) \\ \quad \times \left(1 - \left[\mathrm{r}_{2R} + \mathrm{j}\mathrm{r}_{2I}\right]\mathrm{r}_\mathrm{s}\mathrm{e}^{-\alpha_3}\left[\cos(2\omega\mathrm{T}_3) - \mathrm{j}\sin(2\omega\mathrm{T}_3)\right]\right) \\ \quad -\mathrm{e}^{-\alpha_1}\left[\cos(2\omega\mathrm{T}_1) - \mathrm{j}\sin(2\omega\mathrm{T}_1)\right]\left(\left[\mathrm{r}_{2R} + \mathrm{j}\mathrm{r}_{2I}\right]\right. \\ \quad \left. - \mathrm{r}_\mathrm{s}\mathrm{e}^{-\alpha_2}\left[\cos(2\omega\mathrm{T}_2) - \mathrm{j}\sin(2\omega\mathrm{T}_2)\right]\right) \\ \quad \times \left(\left[\mathrm{r}_{2R} + \mathrm{j}\mathrm{r}_{2I}\right] - \mathrm{r}_\mathrm{s}\mathrm{e}^{-\alpha_3}\left[\cos(2\omega\mathrm{T}_3) - \mathrm{j}\sin(2\omega\mathrm{T}_3)\right]\right) \end{cases} \tag{27}$$

Expansion of this gives:

$$\mathrm{D} = \begin{cases} \left(1 - \mathrm{r}_{2R}\mathrm{r}_\mathrm{s}\mathrm{e}^{-\alpha_2}\cos(2\omega\mathrm{T}_2) - \mathrm{r}_{2I}\mathrm{r}_\mathrm{s}\mathrm{e}^{-\alpha_2}\sin(2\omega\mathrm{T}_2) - \mathrm{j}\mathrm{r}_{2I}\mathrm{r}_\mathrm{s}\mathrm{e}^{-\alpha_2}\cos(2\omega\mathrm{T}_2)\right. \\ \quad \left. + \mathrm{j}\mathrm{r}_{2R}\mathrm{r}_\mathrm{s}\mathrm{e}^{-\alpha_2}\sin(2\omega\mathrm{T}_2)\right) \times \left(1 - \mathrm{r}_{2R}\mathrm{r}_\mathrm{s}\mathrm{e}^{-\alpha_3}\cos(2\omega\mathrm{T}_3)\right. \\ \quad \left. - \mathrm{r}_{2I}\mathrm{r}_\mathrm{s}\mathrm{e}^{-\alpha_3}\sin(2\omega\mathrm{T}_3) - \mathrm{j}\mathrm{r}_{2I}\mathrm{r}_\mathrm{s}\mathrm{e}^{-\alpha_3}\cos(2\omega\mathrm{T}_3) + \mathrm{j}\mathrm{r}_{2R}\mathrm{r}_\mathrm{s}\mathrm{e}^{-\alpha_3}\sin(2\omega\mathrm{T}_3)\right) \\ \quad -\mathrm{e}^{-\alpha_1}\left[\cos(2\omega\mathrm{T}_1) - \mathrm{j}\sin(2\omega\mathrm{T}_1)\right] \\ \times \left[\begin{array}{l} \mathrm{r}_{2R}^2 - \mathrm{r}_{2R}\mathrm{r}_\mathrm{s}\mathrm{e}^{-\alpha_2}\cos(2\omega\mathrm{T}_2) - \mathrm{r}_{2R}\mathrm{r}_\mathrm{s}\mathrm{e}^{-\alpha_3}\cos(2\omega\mathrm{T}_3) \\ \quad + \mathrm{r}_\mathrm{s}^2\mathrm{e}^{-\alpha_2-\alpha_3}\cos(2\omega\mathrm{T}_2)\cos(2\omega\mathrm{T}_3) - \mathrm{r}_{2I}^2 - \mathrm{r}_{2I}\mathrm{r}_\mathrm{s}\mathrm{e}^{-\alpha_2} \\ \quad \times \sin(2\omega\mathrm{T}_2) - \mathrm{r}_{2I}\mathrm{r}_\mathrm{s}\mathrm{e}^{-\alpha_3}\sin(2\omega\mathrm{T}_3) - \mathrm{r}_\mathrm{s}^2\mathrm{e}^{-\alpha_2-\alpha_3} \\ \quad \times \sin(2\omega\mathrm{T}_2)\sin(2\omega\mathrm{T}_3) + \mathrm{j}\mathrm{r}_{2I}\mathrm{r}_{2R} - \mathrm{j}\mathrm{r}_{2I}\mathrm{r}_\mathrm{s}\mathrm{e}^{-\alpha_3}\cos(2\omega\mathrm{T}_3) \\ \quad + \mathrm{j}\mathrm{r}_{2R}\mathrm{r}_\mathrm{s}\mathrm{e}^{-\alpha_2}\sin(2\omega\mathrm{T}_2) - \mathrm{j}\mathrm{r}_\mathrm{s}^2\mathrm{e}^{-\alpha_2-\alpha_3}\sin(2\omega\mathrm{T}_2)\cos(2\omega\mathrm{T}_3) \\ \quad + \mathrm{j}\mathrm{r}_{2I}\mathrm{r}_{2R} - \mathrm{j}\mathrm{r}_{2I}\mathrm{r}_\mathrm{s}\mathrm{e}^{-\alpha_2}\cos(2\omega\mathrm{T}_2) + \mathrm{j}\mathrm{r}_{2R}\mathrm{r}_\mathrm{s}\mathrm{e}^{-\alpha_3}\sin(2\omega\mathrm{T}_3) \\ \quad - \mathrm{j}\mathrm{r}_\mathrm{s}^2\mathrm{e}^{-\alpha_2-\alpha_3}\cos(2\omega\mathrm{T}_2)\sin(2\omega\mathrm{T}_3) \end{array}\right] \end{cases} \tag{28}$$

This is separated into the real and imaginary parts:

$$\mathrm{Re}\,(\mathrm{D}) = \begin{cases} 1 - \left(r_{2R}^2 - r_{2I}^2\right)e^{-\alpha_1}\cos(2\omega T_1) - 2r_{2I}r_{2R}e^{-\alpha_1}\sin(2\omega T_1) \\ - r_s e^{-\alpha_2}\left[r_{2R}\cos(2\omega T_2) + r_{2I}\sin(2\omega T_2)\right] \\ - r_s e^{-\alpha_3}\left[r_{2R}\cos(2\omega T_3) + r_{2I}\sin(2\omega T_3)\right] + \left(r_{2R}^2 - r_{2I}^2\right) \\ \times r_s^2 e^{-\alpha_2-\alpha_3}\cos(2\omega\left[T_2 + T_3\right]) + 2r_{2R}r_{2I}r_s^2 e^{-\alpha_2-\alpha_3} \\ \times \sin(2\omega\left[T_2 + T_3\right]) + r_s e^{-\alpha_1-\alpha_2}\left[r_{2R}\cos\left(2\omega\left[T_1 + T_2\right]\right)\right. \\ \left. + r_{2I}\sin\left(2\omega\left[T_1 + T_2\right]\right)\right] + r_s e^{-\alpha_1-\alpha_3}\left[r_{2R}\cos\left(2\omega\left[T_1 + T_3\right]\right)\right. \\ \left. + r_{2I}\sin\left(2\omega\left[T_1 + T_3\right]\right)\right] \\ - r_s^2 e^{-\alpha_1-\alpha_2-\alpha_3}\cos(2\omega\left[T_1 + T_2 + T_3\right]) \end{cases} \tag{29}$$

$$\mathrm{Im(D)} = \begin{cases} + \left(r_{2R}^2 - r_{2I}^2\right)e^{-\alpha_1}\sin\left(2\omega T_1\right) - 2r_{2I}r_{2R}e^{-\alpha_1}\cos\left(2\omega T_1\right) \\ - r_{2I}r_s\left[e^{-\alpha_2}\cos\left(2\omega T_2\right) + e^{-\alpha_3}\cos\left(2\omega T_3\right)\right] \\ + r_{2R}r_s\left[e^{-\alpha_2}\sin\left(2\omega T_2\right) + e^{-\alpha_3}\sin\left(2\omega T_3\right)\right] \\ + r_{2I}r_s e^{-\alpha_1-\alpha_2}\cos\left(2\omega\left\{T_1 + T_2\right\}\right) - r_{2R}r_s e^{-\alpha_1-\alpha_2} \\ \times \sin\left(2\omega\left\{T_1 + T_2\right\}\right) + r_{2I}r_s e^{-\alpha_1-\alpha_3}\cos\left(2\omega\left\{T_1 + T_3\right\}\right) \\ - r_{2R}r_s e^{-\alpha_1-\alpha_3}\sin\left(2\omega\left\{T_1 + T_3\right\}\right) + 2r_{2R}r_{2I}r_s^2 e^{-\alpha_2-\alpha_3} \\ \times\cos\left(2\omega\left\{T_2 + T_3\right\}\right) + \left(r_{2I}^2 - r_{2R}^2\right)r_s^2 e^{-\alpha_2-\alpha_3}\sin\left(2\omega\left\{T_2 + T_3\right\}\right) \\ + r_s^2 e^{-\alpha_1-\alpha_2-\alpha_3}\sin\left(2\omega\left\{T_1 + T_2 + T_3\right\}\right) \end{cases} \tag{30}$$

One can verify that for a real refractive index n_1 (i.e.: $k_1 = 0$ that gives $r_{2I} = 0$), Eqs. (29) and (30) reduce to Eqs. (12) and (13), respectively. Equations (29) and (30) have to be introduced into Eq. (26) for the exact calculation of an absorbing sample.

2.4.2 Removing the window's fast oscillations

Keeping only the slow varying terms in (D) of Eqs. (29) and (30) give the same simplifications as in Eq. (19). After this operation, one gets:

$$\begin{cases} \mathrm{Re}\,(\mathrm{D}) = 1 - \left(r_{2R}^2 - r_{2I}^2\right)e^{-\alpha_1}\cos\left(2\,\omega\,T_1\right) - 2r_{2I}r_{2R}e^{-\alpha_1}\sin\left(2\,\omega\,T_1\right) \\ \mathrm{Im(D)} = \left(r_{2R}^2 - r_{2I}^2\right)e^{-\alpha_1}\sin\left(2\,\omega\,T_1\right) - 2r_{2I}r_{2R}e^{-\alpha_1}\cos\left(2\,\omega\,T_1\right) \end{cases} \tag{31}$$

This equation being different than Eq. (18) indicates that the interference patterns obtained from absorbing samples are different from non absorbing ones. Equation (31) gives after rearrangement:

$$\begin{aligned} \mathrm{Re}^2\,(\mathrm{D}) + \mathrm{Im}^2(\mathrm{D}) = 1 - 2\left(r_{2R}^2 - r_{2I}^2\right)e^{-\alpha_1}\cos\left(2\,\omega\,T_1\right) \\ -4r_{2I}r_{2R}e^{-\alpha_1}\sin\left(2\,\omega\,T_1\right) + \left(r_{2R}^2 + r_{2I}^2\right)^2 e^{-2\alpha_1} \end{aligned} \tag{32}$$

The reflection coefficient complex nature generated by an absorbing sample makes Eq. (32) different from the denominator in Eq. (19). In Eq. (32) we have

$$\mathrm{r}_{2R}^2 - \mathrm{r}_{2I}^2 = \frac{\left(n_2^2 - n_1^2\right)^2 + k_1^4 - 6n_2^2k_1^2 + 2n_1^2k_1^2}{\left[(n_2 + n_1)^2 + k_1^2\right]^2} \tag{33}$$

$$\left(\mathrm{r}_{2R}^2 + \mathrm{r}_{2I}^2\right)^2 = \frac{\left[\left(n_2^2 - n_1^2\right)^2 + k_1^4 + 2n_2^2k_1^2 + 2n_1^2k_1^2\right]^2}{\left[(n_2 + n_1)^2 + k_1^2\right]^4} \tag{34}$$

The terms in Eqs. (33) and (34) are different from that in Eq. (19) in which the complex values of the reflection coefficient was ignored. From Eq. (25) we have:

$$\begin{aligned}\left\|1 - \mathrm{r}_2^{*2}\right\|^2 &= \left\|1 - \left(\mathrm{r}_{2R} + \mathrm{j}\mathrm{r}_{2I}\right)^2\right\|^2 = \left\|1 - \mathrm{r}_{2R}^2 + \mathrm{r}_{2I}^2 - 2\mathrm{j}\mathrm{r}_{2R}\mathrm{r}_{2I}\right\|^2 \\ &= \left(1 - \mathrm{r}_{2R}^2 + \mathrm{r}_{2I}^2\right)^2 + 4\mathrm{r}_{2R}^2\mathrm{r}_{2I}^2 \end{aligned} \tag{35}$$

$$\left\|1 - \mathrm{r}_2^{*2}\right\|^2 = 1 + \mathrm{r}_{2R}^4 + \mathrm{r}_{2I}^4 - 2\mathrm{r}_{2R}^2 + 2\mathrm{r}_{2I}^2 + 2\mathrm{r}_{2R}^2\mathrm{r}_{2I}^2 \tag{36}$$

The transmission of an absorbing sample between two transparent windows is evaluated with Eqs. (26), (32), and (36).

2.4.3 Integration over sample thickness variations

Depending on the experimental setup, interferences due to the sample are partly damped because of thickness variations [18]. This comes from: (i) lack of parallelism of the windows; (ii) window deformations due to pressure variations; (iii) window roughness; or (iv) a combination of these. Integrating the transmitted intensity over a thickness range takes care of these variations. Numerical integration was proposed [18] that is not easy to handle because of the approximations used. However, analytical integration is possible with approximations evaluated below.

Interference fringes come from oscillating terms in Eqs. (26) and (32). Since the other terms vary slowly with the sample thickness their average value can be used. Integration over sample thickness ℓ_1 will affect the trigonometric functions in Eqs. (26) and (32). Analytical integration of Eq. (26) necessitates the replacement of the denominator $[\mathrm{Re}^2(\mathrm{D}) + \mathrm{Im}^2(\mathrm{D})]$ by an easily integrable function. This is done by a development in series. From Eq. (32), the denominator in Eq. (26) $[\mathrm{Re}^2(\mathrm{D}) + \mathrm{Im}^2(\mathrm{D})]$ is written as $1 + Q$ where Q is:

$$\begin{aligned} Q = &-2\left(\mathrm{r}_{2R}^2 - \mathrm{r}_{2I}^2\right)\mathrm{e}^{-\alpha_1}\cos\left(2\omega\mathrm{T}_1\right) - 4\mathrm{r}_{2I}\mathrm{r}_{2R}\mathrm{e}^{-\alpha_1}\sin\left(2\omega\mathrm{T}_1\right) \\ &+ \left(\mathrm{r}_{2R}^2 + \mathrm{r}_{2I}^2\right)^2\mathrm{e}^{-2\alpha_1} \end{aligned} \tag{37}$$

With a sample thickness variation of $\pm\delta$ we have $-1 < Q < 1$. $1/(1+Q)$ developed with the series $= 1-Q + Q^2-Q^3\ldots$ gives for Eq. (26):

$$\mathrm{T} \approx \left(1-\mathrm{r_s^2}\right)^2 \left\|1-\mathrm{r_2^{*2}}\right\|^2 \mathrm{e}^{-(\alpha_1+\alpha_2+\alpha_3)} \times \left[1-Q\left(\ell_1\right)+Q^2\left(\ell_1\right)-Q^3\left(\ell_1\right)\cdots\right] \tag{38}$$

An analytical form for the integration of Eq. (38) is possible giving an approximation the validity of which must be evaluated. Appendix A gives a step by step development of the integration of Eq. (38). Assuming a square box distribution of the sample thickness (a uniform distribution over the sample area), the analytical equation obtained from the integration up to the 6th harmonics of the fundamental modulating period due to the sample thickness variation ($\pm\delta$) is given by:

$$\begin{aligned}
&\frac{1}{2\delta}\int_{\ell_1-\delta}^{\ell_1+\delta} \mathrm{T}\mathrm{d}\ell_1 \approx \left(1-\mathrm{r_s^2}\right)^2 \left\|1-\mathrm{r_2^{*2}}\right\|^2 \mathrm{e}^{-(\alpha_1+\alpha_2+\alpha_3)} \times \frac{1}{1-\left(\mathrm{r_{2R}^2}+\mathrm{r_{2I}^2}\right)^2\mathrm{e}^{-2\alpha_1}} \\
&\times \left\{\begin{array}{l}
1 \\
+\frac{\sin(400\pi\tilde{\nu}n_1\delta)}{200\pi\tilde{\nu}n_1\delta}\mathrm{e}^{-\alpha_1}\left[\left(\mathrm{r_{2R}^2}-\mathrm{r_{2I}^2}\right)\cos\left(2\omega\mathrm{T}_1\right)+2\mathrm{r_{2I}}\mathrm{r_{2R}}\sin\left(2\omega\mathrm{T}_1\right)\right] \\
+\frac{\sin(800\pi\tilde{\nu}n_1\delta)}{400\pi\tilde{\nu}n_1\delta}\mathrm{e}^{-2\alpha_1}\left\{\left[\left(\mathrm{r_{2R}^2}-\mathrm{r_{2I}^2}\right)^2-4\mathrm{r_{2I}^2}\mathrm{r_{2R}^2}\right]\cos\left(4\omega\mathrm{T}_1\right)\right. \\
\qquad\left.+4\mathrm{r_{2I}}\mathrm{r_{2R}}\left(\mathrm{r_{2R}^2}-\mathrm{r_{2I}^2}\right)\sin\left(4\omega\mathrm{T}_1\right)\right\} \\
+\frac{\sin(1200\pi\tilde{\nu}n_1\delta)}{600\pi\tilde{\nu}n_1\delta}\mathrm{e}^{-3\alpha_1}\left\{\left(\mathrm{r_{2R}^2}-\mathrm{r_{2I}^2}\right)\left[\left(\mathrm{r_{2R}^2}-\mathrm{r_{2I}^2}\right)^2-12\mathrm{r_{2I}^2}\mathrm{r_{2R}^2}\right]\cos\left(6\omega\mathrm{T}_1\right)\right. \\
\qquad\left.+2\mathrm{r_{2I}}\mathrm{r_{2R}}\left[3\left(\mathrm{r_{2R}^2}-\mathrm{r_{2I}^2}\right)^2-4\mathrm{r_{2I}^2}\mathrm{r_{2R}^2}\right]\sin\left(6\omega\mathrm{T}_1\right)\right\} \\
+\frac{\sin(1600\pi\tilde{\nu}n_1\delta)}{800\pi\tilde{\nu}n_1\delta}\mathrm{e}^{-4\alpha_1}\left\{\begin{array}{l}\left[\left(\mathrm{r_{2R}^2}-\mathrm{r_{2I}^2}\right)^4+16\mathrm{r_{2I}^4}\mathrm{r_{2R}^4}-24\left(\mathrm{r_{2R}^2}-\mathrm{r_{2I}^2}\right)^2\mathrm{r_{2I}^2}\mathrm{r_{2R}^2}\right] \\ \times\cos\left(8\omega\mathrm{T}_1\right)+8\left(\mathrm{r_{2R}^2}-\mathrm{r_{2I}^2}\right) \\ \times\mathrm{r_{2I}}\mathrm{r_{2R}}\left[\left(\mathrm{r_{2R}^2}-\mathrm{r_{2I}^2}\right)^2-4\mathrm{r_{2I}^2}\mathrm{r_{2R}^2}\right]\sin\left(8\omega\mathrm{T}_1\right)\end{array}\right\} \\
+\frac{\sin(2000\pi\tilde{\nu}n_1\delta)}{1000\pi\tilde{\nu}n_1\delta}\mathrm{e}^{-5\alpha_1}\left\{\begin{array}{l}\left(\mathrm{r_{2R}^2}-\mathrm{r_{2I}^2}\right)\left[\left(\mathrm{r_{2R}^2}-\mathrm{r_{2I}^2}\right)^4-40\left(\mathrm{r_{2R}^2}-\mathrm{r_{2I}^2}\right)^2\mathrm{r_{2I}^2}\mathrm{r_{2R}^2}\right. \\ \qquad\left.+80\mathrm{r_{2I}^4}\mathrm{r_{2R}^4}\right]\cos\left(10\omega\mathrm{T}_1\right) \\ +2\mathrm{r_{2I}}\mathrm{r_{2R}}\times\left[5\left(\mathrm{r_{2R}^2}-\mathrm{r_{2I}^2}\right)^4-40\left(\mathrm{r_{2R}^2}-\mathrm{r_{2I}^2}\right)^2\mathrm{r_{2I}^2}\mathrm{r_{2R}^2}\right. \\ \qquad\left.+16\mathrm{r_{2I}^4}\mathrm{r_{2R}^4}\right]\sin\left(10\omega\mathrm{T}_1\right)\end{array}\right. \\
+\frac{\sin(2400\pi\tilde{\nu}n_1\delta)}{1200\pi\tilde{\nu}n_1\delta}\mathrm{e}^{-6\alpha_1}\left\{\begin{array}{l}\left[\left(\mathrm{r_{2R}^2}-\mathrm{r_{2I}^2}\right)^6-60\left(\mathrm{r_{2R}^2}-\mathrm{r_{2I}^2}\right)^4\mathrm{r_{2I}^2}\mathrm{r_{2R}^2}\right. \\ \quad\left.+240\left(\mathrm{r_{2R}^2}-\mathrm{r_{2I}^2}\right)^2\mathrm{r_{2I}^4}\mathrm{r_{2R}^4}-64\mathrm{r_{2I}^6}\mathrm{r_{2R}^6}\right]\cos\left(12\omega\mathrm{T}_1\right) \\ +\left[12\left(\mathrm{r_{2R}^2}-\mathrm{r_{2I}^2}\right)^5\mathrm{r_{2I}}\mathrm{r_{2R}}-160\left(\mathrm{r_{2R}^2}-\mathrm{r_{2I}^2}\right)^3\mathrm{r_{2I}^3}\mathrm{r_{2R}^3}\right. \\ \quad\left.+192\left(\mathrm{r_{2R}^2}-\mathrm{r_{2I}^2}\right)\mathrm{r_{2I}^5}\mathrm{r_{2R}^5}\right]\sin\left(12\omega\mathrm{T}_1\right)\end{array}\right. \\
+f\left(\cos\left(2p\omega\mathrm{T}_1\right),\sin\left(2p\omega\mathrm{T}_1\right),\ p>6\right)
\end{array}\right.
\end{aligned} \tag{39}$$

The big advantage of this analytical form is that numerical applications are easy and results are quickly obtained contrary to numerical integration. The maximum thickness deviation from the average value, δ, is the important parameter of this integration. These calculations can be made in a spreadsheet program where the parameter can be varied rapidly.

Equation (39) is useful for handling sample thickness variations, knowing that wedge shaped cells are often used for determining sample extinction coefficients [23]. In these, even though the window plates are very flat it is impossible to obtain a uniform sampling cavity [33]. Nonetheless, for this and other situations Eq. (39) gives excellent results for the determination of the sample optical properties.

3 Chemicals, solutions, and IR measurements

The IR measurements were obtained with a model 510P Nicolet FTIR spectrometer with a DTGS (deuterium triglycine sulfate) detector. The samples were contained in transmission cells with Si, ZnSe and BaF_2 windows 4 mm thick separated by 25, 50, 100, and 1800 μm spacers. The spectra obtained at 27.1 °C come from an accumulation of 100 scans or more at 2 cm^{-1} resolution. The data are transferred to a spreadsheet program for numerical calculations. Compensation for the windows absorption was made with single window absorption spectra after removing their insertion loss. This is obtained at high frequency where the windows do not absorb.

4 Results and discussion

4.1 Accuracy of the integration

The accuracy of the approximation up to the 6th harmonic is evaluated in a situation where lower order approximations failed for water sandwiched between Si windows. This pair creates high amplitude reflections due to the great difference in the refractive indices. Furthermore, water has very broad intense bands and low intensity ones. Absorption of water films 2.2 μm thick was calculated with Eqs. (26) and (32) for Si windows (4 mm thickness). These equations deal with uniform films. The spectra were also calculated with the approximate Eq. (39) for which the thickness variation was arbitrarily put close to zero: 0.001 μm (i.e. $\delta \rightarrow 0$). The results are plotted in Fig. 2a. The difference (right scale) between the two methods is less than $\pm 10^{-4}$ absorbance unit (AU). These results indicate that the approximate method gives sufficiently good results. In the strong absorption regions ($\sim$3,400 cm^{-1}), the difference between the two methods is null because the strong absorption damps the signal. In these regions multiple reflections do not occur. The overall result indicates that the approximation equation is valid for reflection ratio up to 0.60.

In Fig. 2a we observe in the water low absorption regions situated between 4,800–3,800 and 2,800–2,000 cm^{-1} strong distortion attributed to multiple reflections in the water films. These are clear examples of the influence of multiple reflections taking place at the window interfaces. This justifies the effort of the present work to circumscribe this phenomenon.

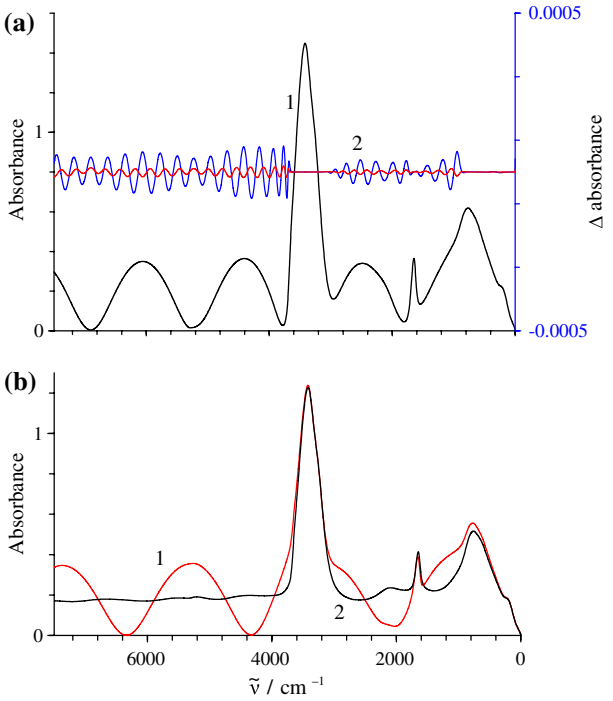

Fig. 2 Calculated water film intensities between two Si windows excluding air/window reflection loss. **a** With exact Eqs. (26) and (32) and approximate Eq. (39) up to the 5th and 6th harmonics for a uniform 2.2 μm film: (*1, black*) (Note: the curves are superimposed); and (*2*) difference between exact and approximate calculation: 5th (*blue*, biggest differences) and 6th (*red*, smallest differences) harmonics. **b** For parallel (*1, red*), and edge 1.8 μm ($\delta = 1.5\,\mu$m) film (*2, black*) with Eq. (39). (Color figure online)

4.2 Effect of sample thickness variation (wedge shaped cell)

The use of a wedge shaped cell was proposed as a means to reduce the distortion created by strong internal reflections inside the sample by retrieving the Beer–Lambert's absorption slope: absorption as a function of sample thickness [23]. However, this does not eliminate the perturbations generated by the internal multiple reflections. Equations developed in the theoretical section (section II D) were used to verify that the experimental spectrum is related to the film's physical dimensions and its optical characteristics.

The effect of the sample thickness variation is illustrated by the two spectra in Fig. 2b. Spectrum (1) is from a uniform 1.8 μm water film and spectrum (2) from a film that varies linearly from 0.3 to 3.3 μm giving an average of 1.8 μm. The first spectrum is strongly distorted while second is apparently not distorted. This is a false impression because the base line suffers a large shift in the low absorption regions (7,900–3,900 and 2,800–2,400 cm^{-1}). Attempts to correct the baseline by placing it at zero in the non absorbing regions will give negative absorption in the low frequency region. This will result in an incorrect spectrum. Although the base lines shift procedure is often used spectrum (2) in Fig. 2b clearly illustrates that it is unacceptable.

When only MIR transmission measurements are obtained, this phenomenon pass unnoticed because the negative part in the FIR has not been obtained. However, a close look at spectrum (2) indicates that a sinusoidal remains in the non absorbing regions. Nonetheless, the absorbing bands are perturbed by this phenomenon which affects the band intensity measurements. Moreover, the band shape being distorted makes the bands difficult to simulate by band fit procedures. When the baseline is arbitrary displaced, the intensity measurements and simulations give poor results.

4.3 Comparison between results obtained for liquid water with the equations proposed and those of Zelsmann

In our IR study of liquid water and aqueous mixtures we used the ATR technique with a ZnSe crystal which easily gives good reproducible spectra [1–7]. However, since this crystal absorbs below 650 cm^{-1} the low frequency region is inaccessible. To obtain the spectra of light and heavy water in this region Zelsmann measured the transmission spectra of a 19.3 μm water film between two Si windows [22]. Because of its high refractive index which gives rise to multiple reflections in the water sample it was necessary to redo some calculations to extract the water optical properties in the 450–50 cm^{-1} region. Trace (1) in Fig. 3a gives the results of Zelsmann and in trace (2) that calculated with Eq. (39) up to the 6th harmonics by using the water k and n values given in ref. [22]. Figure 3a shows that the two curves are almost coincident with, however, some differences. These are plotted with an expanded scale in Frame (b). In the low frequency region this plot gives only a difference of ±0.05 AU but since the signal is low it gives a 25% error. We cannot ignore this, especially when trying to concatenate data from different spectral regions using different optical materials and techniques. For example, Fourier transformation of data with a sharp step will generate a sinusoidal train in the spectra. One of the objectives of this paper is to provide trouble free equations that will avoid such mismatches.

4.4 IR spectra of BaF_2, ZnSe and Si windows

Figure 4 shows the transmission spectra in AU of BaF_2 (1), ZnSe (2), and Si (3) windows with their respective insertion loss. The spectra are flat with very weak bands in the 1,600–1,400 cm^{-1} region for BaF_2 and stronger ones for ZnSe below 700 cm^{-1}. For these, small remaining fluctuations of less than 5 mAU may originate from micro-impurities, surface imperfections, or a combination of both. However, these windows absorb in the FIR rendering them useless for obtaining spectra in that region. Nevertheless, their evaluations are useful for understanding the multiple reflection phenomena and serve as a reference for their transparency regions which are from 7,000 to 700 and 7,000 to 500 cm^{-1} for BaF_2 and ZnSe, respectively.

The Si window (Fig. 4, spectrum 3) is both a useful and difficult window. Its transparency range is between 9,000 and 10 cm^{-1} which makes it a good candidate for the FIR region. However, it has moderate absorption below 1,500 cm^{-1} and strong bands near 600 cm^{-1}. Sample bands situated downstream from this strong band will be perturbed by it. Furthermore, the Si high refractive index (3.4223 @ 5 μm) will

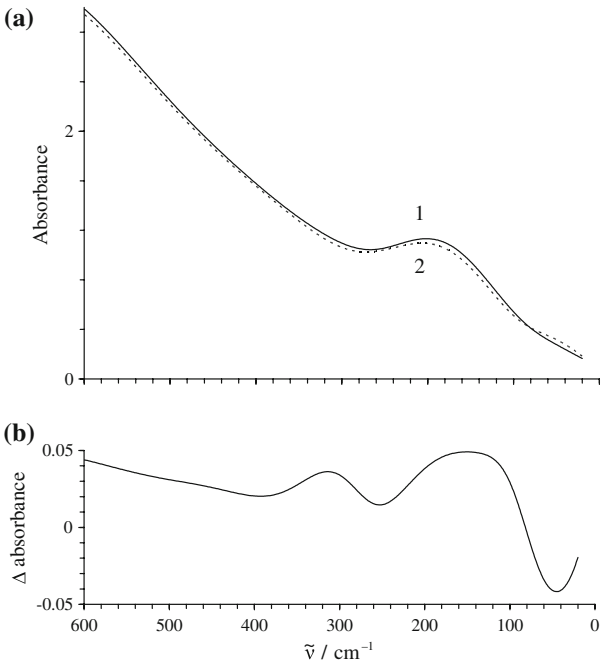

Fig. 3 Calculated 19.3 μm water film between two Si windows excluding window reflection loss. **a** With corrected Zelsmann's equation (see text) (*1, full line*) and with Eq. (39) and $\delta = 0.001\,\mu\text{m}$ (*2, dotted line*). **b** Difference between (*1*) and (*2*) with a scale expansion of 30

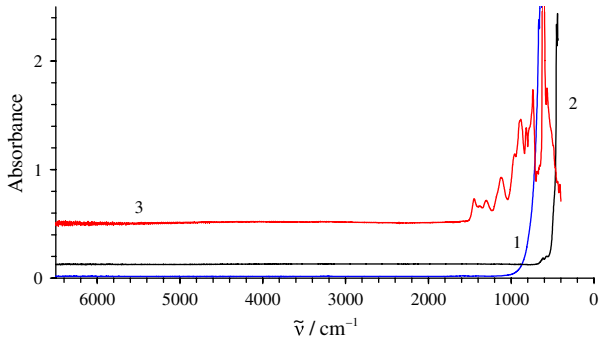

Fig. 4 IR spectra of 4 mm windows: (*1, blue*) BaF_2; (*2, black*) ZnSe; and (*3, red*) Si (including reflection loss). (Color figure online)

produce high reflection losses at its surface. This will generate strong interference fringes in a boxcar cell. Moreover, from the Kramers–Kronig relationship between the real (n) and imaginary (k) parts of the refractive index, the real part will change close to an absorption band. This is the case for ZnSe whose refractive index real part was reported down to $500\,\text{cm}^{-1}$ ($n = 2.43$ @ $5\,\mu\text{m}$ and 2.3 @ $20\,\mu\text{m}$) [34,35]. The refractive indices of BaF_2 also decreases below $1{,}000\,\text{cm}^{-1}$ [34,35]. However, since

we do not have the refractive index values of BaF_2 and Si windows near their strong absorption we considered them constant at respectively 1.46 and 3.422 in their usefulness region. That is outside the perturbation regions of the strong absorption. However, the limit of these regions has to be delimitated so as to be as small as possible.

4.5 Thick layer oscillations

The problem of the multiple reflections in IR cells for liquid or gas samples cannot be discarded but needs special care. It is generally claimed that for sufficiently thick samples or windows, the multiple reflections are eliminated because they are below the spectrum resolution [22]. The oscillations generated by internal multiple reflections cannot be followed adequately because the spectrum is undersampled: the sampling interval is greater than the oscillation spacing. However, they may create an aliasing effect that corresponds to a lower beat period related to the difference between the oscillation frequency and the sampling frequency [18,36]. Furthermore, contrary to a dispersive instrument a FTIR spectrometer has no filter (except the interferogram apodization) to damp the phenomenon. As an example a 0.180 cm air sample between two Si windows gives spectra (2) in Fig. 5 in which the crosses indicate the sampling

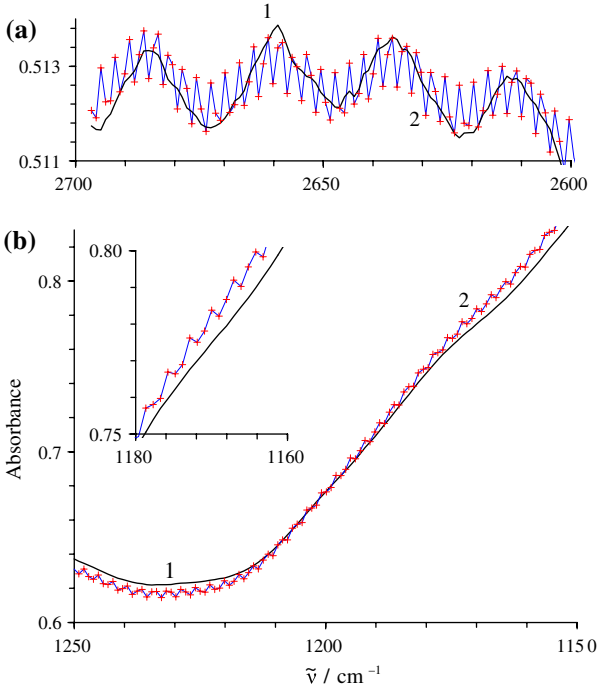

Fig. 5 Experimental absorption IR spectra (including reflection loss) of (*1, black*) 8 mm Si window; (*2, blue* and *red* crosses) 1.8 mm air path between two 4 mm Si windows. **a** Region without window band absorption and **b** region with window band absorption. (Color figure online)

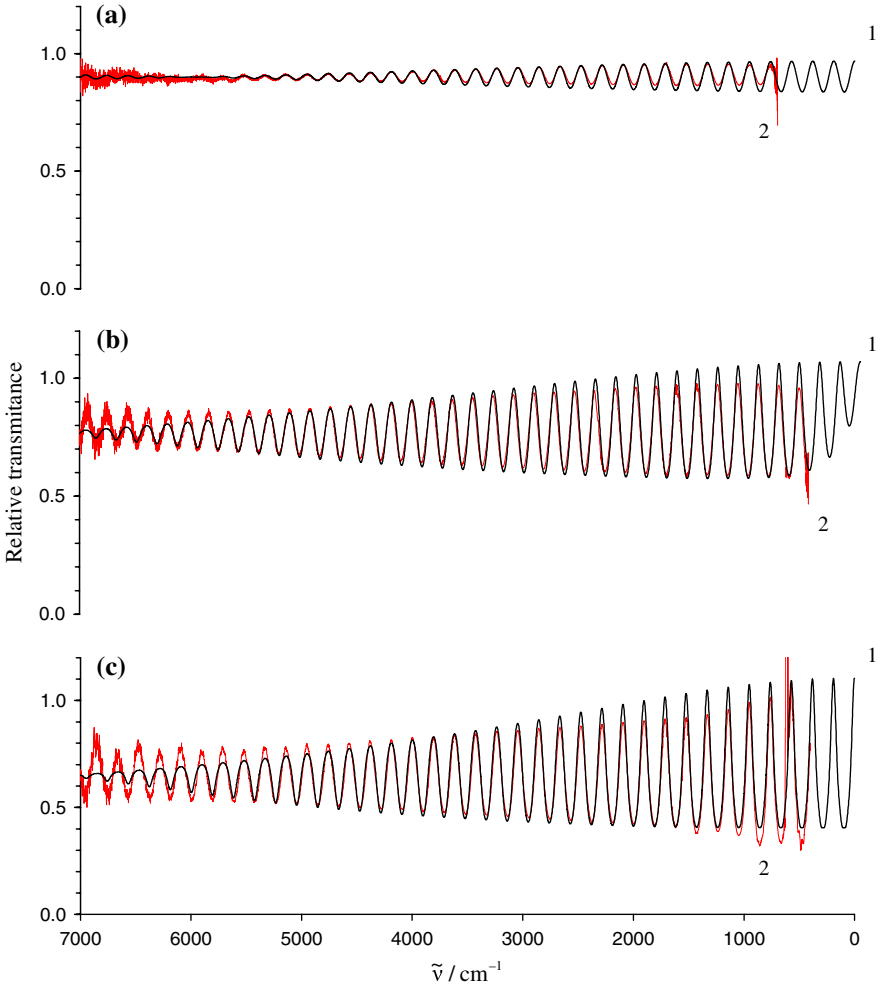

Fig. 6 Comparison between calculated (*1, black*) and experimental (*2, red*) relative transmittance of air between two windows: **a** BaF_2, **b** ZnSe, and **c** Si. Thickness are 26.25 μm ($\delta = 0.42$ μm); 27.35 μm ($\delta = 0.34$ μm); 26.26 μm ($\delta = 0.35$ μm), respectively. (Color figure online)

points with 0.96 cm^{-1} sampling interval. In the non-absorbing and absorbing regions the oscillations are separated by ∼2.78 cm^{-1} in frames (a) and (b).[1] Since the sampling interval is 0.96 cm^{-1}, the oscillations are readily observed. However, the amplitude of these oscillations is reduced compared to that of Fig. 6c. This is due to (i) the filtering effect of the apodization used in the Fourier transform of the interferograms; and (ii) to window surfaces irregularities.

[1] The distance between two oscillations is: $\Delta\tilde{\nu} = 1/(2n\ell)$ where the "2" is for the two faces, n is the refractive index, and ℓ for the distance between the faces. For air $n = 1.00$ and $\ell = 0.18$ cm $\Delta\tilde{\nu} = 2.78$ cm^{-1}. For one Si window $n = 3.42$ and $\ell = 0.40$ cm $\Delta\tilde{\nu} = 0.37$ cm^{-1}.

For a single Si window (8 mm) curve (1) in Fig. 5 illustrates the transmission spectrum obtained. The multiple reflections should produce oscillations of 0.37 cm^{-1} (see foot note 1) but since these are outside the sampling interval they are not observed except for small remaining fluctuations. However, very low amplitude oscillations (<0.002 transmission units equal to <0.002 absorbance units) of around 24 cm^{-1} period are observed in both curves (1) and (2). These oscillations displayed in spectrum (1) of Fig. 5 are weak (<0.002 AU peak to peak). The reasons for this are: (i) window surface roughness whose transmitted signal integrates different thicknesses (see Appendix D for details); (ii) window flatness; (iii) window parallelism; and (iv) window absorption. Hence the resonance inside each window is reduced. For thick windows these oscillations are difficult to observe experimentally but they can modify the spectra.

4.6 Oscillation pattern due to air sample

Since it is easy to obtain the transmission spectra of air gaps between two windows, we use them to validate the transmission equations proposed in the present work. Figure 6 frames (a), (b), and (c) display the relative transmission spectra of a 25 μm air sample taken between, BaF_2, ZnSe, and Si windows, respectively. These show that the interference intensity pattern (i) increases from BaF_2 to Si and (ii) is damped with increasing frequency. The first property is in good agreement with the air-window reflection coefficient that increases (0.035, 0.177 and 0.300, respectively) with the window refractive indices: BaF_2, 1.462; ZnSe, 2.45; and Si, 3.42. The null absorption of air should give a constant amplitude interference pattern. However, this is not the case because the windows are not: (i) perfectly parallel; (ii) perfectly flat; or (iii) perfectly polished. Integrating the transmission with Eq. (39) over the sample thickness variation will take care of problems (i) and (ii). The calculated spectra in Fig. 6 were fitted to the experimental ones by adjusting two parameters: average sample thickness and sample thickness variation. For the three window pairs, the average thickness of the 25 μm spacer was 26.62 ± 0.75 μm and thickness variation (δ) 0.37 ± 0.05 μm.

With the above parameters the spectra were recalculated. Figure 6 indicates a good match between calculated and experimental spectra. The small remaining mismatch could be due to (i) sample thickness distribution that may be different from a square box; (ii) the lack of uniformity of the source beam; (iii) the variation of the window refractive index; or (iv) a combination of these. Measurements with 50 and 100 μm air gaps were also recorded. These compared satisfactorily with calculations. Defects located at strong window absorptions (700, 470, 600 cm^{-1}, for BaF_2, ZnSe and Si, respectively) are related to spectrometer inaccuracy.

Notwithstanding the small remaining mismatches the results of Fig. 6 indicate that the oscillation damping effect with increasing frequency can be assigned to sample thickness variations in the light beam.

4.7 Air samples and fringes

Figures 7, 8, 9 show the transmission spectra of air samples sandwiched between BaF_2, ZnSe, and Si windows, respectively. The experimental spectra were obtained for three

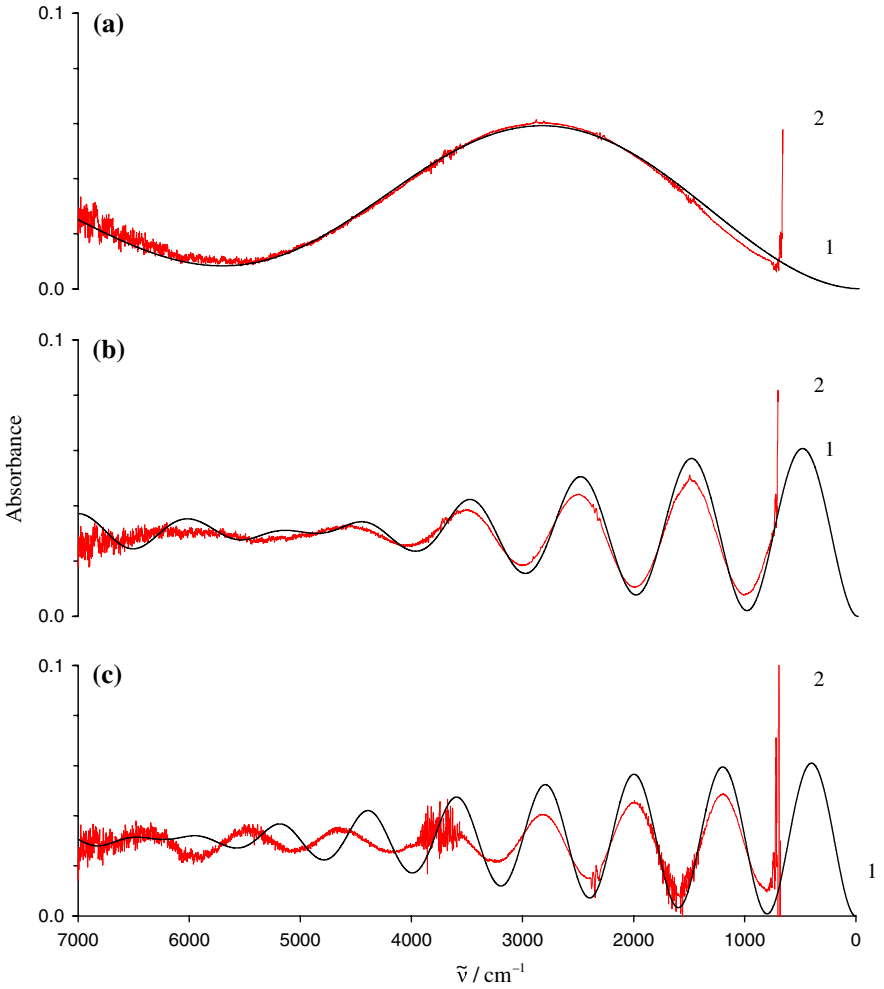

Fig. 7 Comparison between calculated (*1, black*) and experimental (*2, red*) spectra of air between two BaF_2 windows with different thickness: **a** 0.86 μm ($\delta = 0.18$ μm); **b** 5.00 μm ($\delta = 0.50$ μm); **c** 6.25 μm ($\delta = 0.40$ μm). Window reflection loss and absorption are subtracted. (Color figure online)

thicknesses and compared with calculated ones with Eq. (39) that were developed up to the 6th harmonic.

4.7.1 BaF_2 windows

Figure 7a presents a very good match for an air gap thickness: 0.86 μm ($\delta = 0.18$ μm). The oscillations are properly reproduced along with the amplitude decrease. The base line of the experimental spectrum was corrected with a linear function.

Figure 7b showing an air gap of 5.00 μm ($\delta = 0.50$ μm) illustrates the good agreement between calculated and measured traces. However, the experimental oscillations

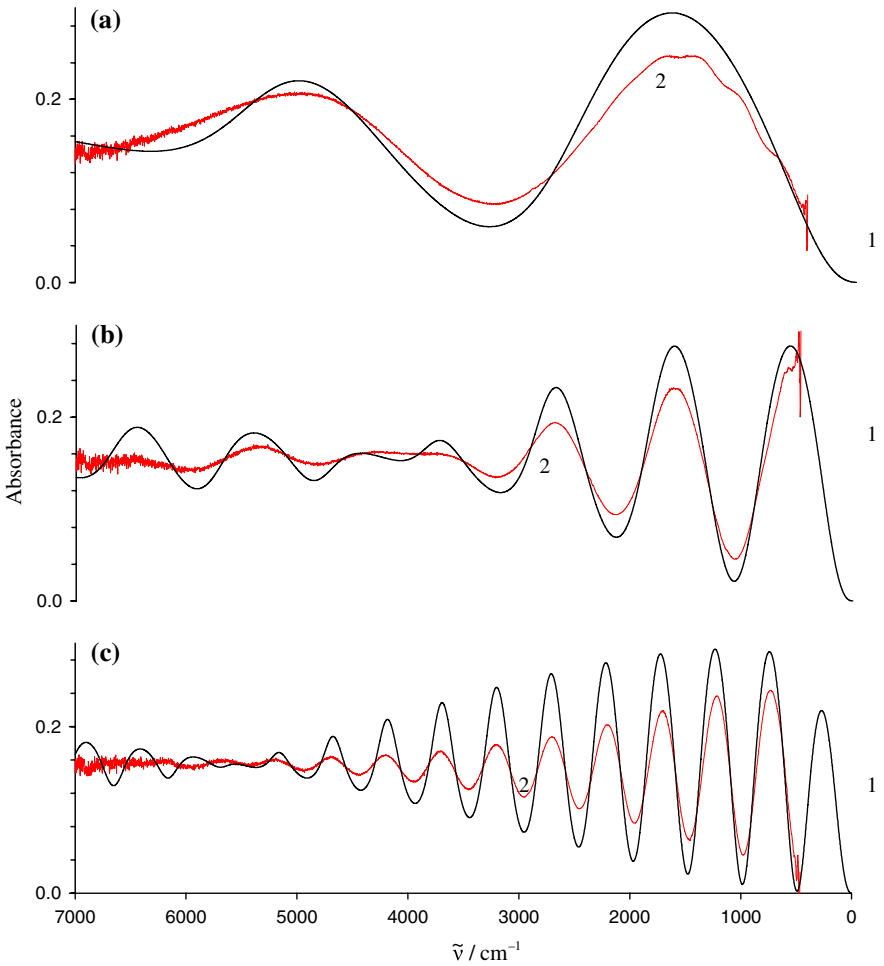

Fig. 8 Comparison between calculated (*1, black*) and experimental (*2, red*) spectra of air between two ZnSe windows with different thickness: **a** 1.47 μm ($\delta = 0.35$ μm); **b** 4.65 μm ($\delta = 0.60$ μm); **c** 10.15 μm ($\delta = 0.45$ μm). Window reflection loss and absorption are subtracted. (Color figure online)

are slightly weaker than the calculated ones. This is attributed to some reflection coherence loss due to the surface roughness.

Figure 7c is for an air gap of 6.25 μm ($\delta = 0.40$ μm) that shows a similar pattern as that in Fig. 7b. However, at high frequency we notice that the experimentally observed oscillation intervals increase. The present calculations cannot account for these.

4.7.2 ZnSe windows

Figure 8 frames (a), (b), and (c) show the transmission of thin air gaps of 1.47 μm ($\delta = 0.35$ μm), 4.65 μm ($\delta = 0.60$ μm), and 10.15 μm ($\delta = 0.45$ μm), respectively. The match between calculated and experimental results are good, however, the interfer-

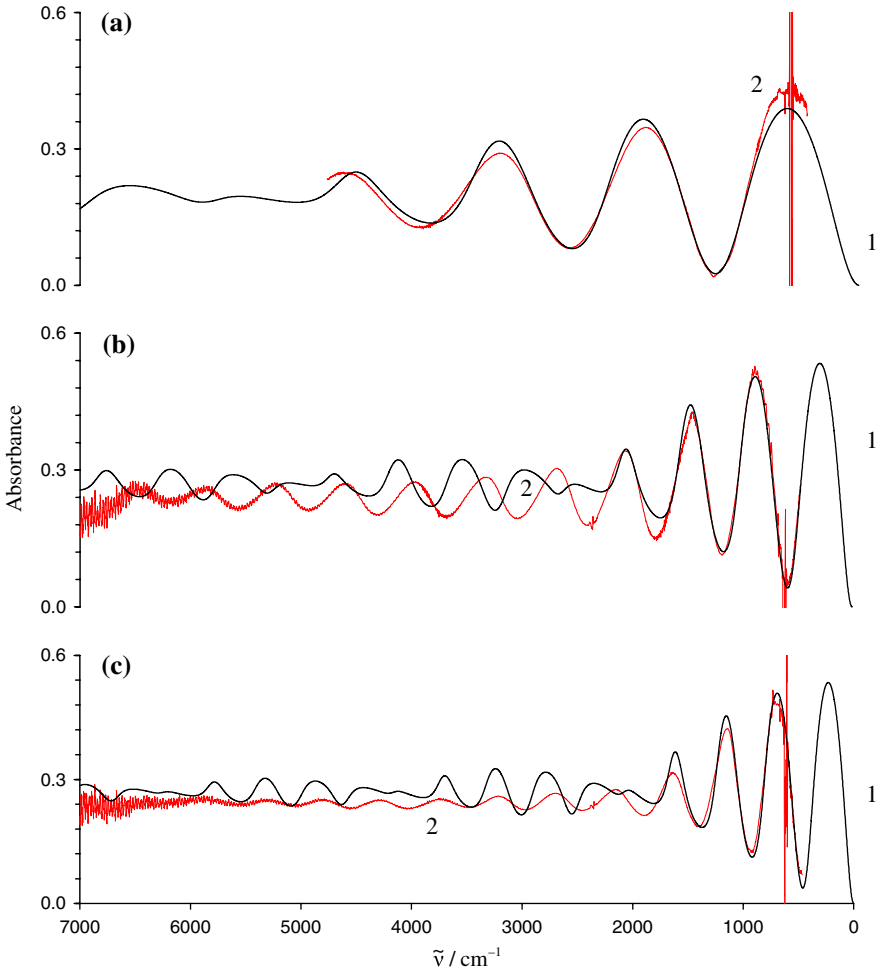

Fig. 9 Comparison between calculated (*1, black*) and experimental (*2, red*) spectra of air between two Si windows with different thickness: **a** 3.85 μm ($\delta = 0.45\,\mu$m); **b** 8.5 μm ($\delta = 1.0\,\mu$m); **c** 10.8 μm ($\delta = 1.2\,\mu$m). Window reflection loss and absorbtion are subtracted. (Color figure online)

ence amplitudes are a little lower than the calculated ones. The causes of these small mismatches are the same as for BaF_2 windows.

The beat feature (amplitude decrease followed by a further increase) is readily observed in the experimental spectrum in Fig. 8b. The fair match between calculated and experimental spectra indicates that this feature is attributed to the air gap thickness variations. In Fig. 8c the intensity decrease below 1,000 cm^{-1} of the calculated fringes comes from the diminishing ZnSe refractive index [34,35].

4.7.3 Si windows

Figure 9 frames (a), (b), and (c) show the transmission of a thin air gap of 3.90 μm ($\delta = 0.45\,\mu$m), 8.5 μm ($\delta = 0.75\,\mu$m), and 10.80 μm ($\delta = 1.20\,\mu$m), respectively. The

oscillation patterns are maintained throughout with some small resonance beats in both calculated and experimental spectra. The match is good for the three lower frequency oscillations but is lost for higher frequencies. The cause of mismatches is the same as for BaF_2 and ZnSe increased by the higher refractive index of Si. Furthermore Si has OH groups adsorbed to its surface that may influence the window's reflectivity.

Figure 9 that illustrate the Si windows absorption shows some unexpected features that the equations developed here do not explain. Instead of the oscillation beat (damping followed by an intensity increase) expected the oscillation shape and interval change at the higher frequencies. Figure 9a shows a variation in the oscillation period near 3,500 cm^{-1}. Similarly, Fig. 9b and c show oscillation mismatches that start near 2,000 cm^{-1}. This is due to (i) the weighing function used for thickness variation integration. We choose a uniform thickness distribution which may not be exact; (ii) the incident light may not be exactly normal; and (iii) the surface roughness can attenuate differently the interferences at different frequencies and periods.

Notwithstanding the small mismatches between calculated and experimental spectra obtained for the three windows Eq. (39) developed up to the 6th harmonic are adequate and sufficient for our needs which are mainly in the FIR. Recall that the match between calculated and experimental spectra is very good up to 2,000 cm^{-1}.

4.8 Liquid samples and fringes

Figure 10 illustrates the comparison between the calculated and experimental spectra of liquid D_2O between two windows with a pathlength of near 25 μm. With this pathlength the stretch bands ($\sim$2,400 cm^{-1}) in frame (a) and (b) are stronger than 2.5 AU which is the limit of the detectivity of our system. To the water sample absorption, the reflection losses must be added: 0.05 and 0.25 AU for BaF_2 and ZnSe windows, respectively. The deformation bands ($\sim$1,210 cm^{-1}) are slightly stronger than 2.5 absorbance. Notwithstanding these limits, the rest of the spectra clearly show the validity of the calculated spectra. With the BaF_2 windows (27.6 μm ($\delta = 0.6\,\mu m$) sample thickness), the match between calculated (1) and experimental (2) spectra is almost perfect. Only two mismatches occur: one band near 3,400 cm^{-1} and a shoulder near 1,470 cm^{-1} are present in the experimental spectra (2) and not in the calculated one (1). These come from a small amount of HDO in the D_2O sample used whereas the calculated spectrum one is made with pure D_2O only. Figure 10a also shows interference fringes in the 5,000–4,000 cm^{-1} region, where absorption is very low. These fringes ($\sim$140 cm^{-1} spacing) point out the fact that interferences are present in low absorption region and therefore must not be neglected in the NIR region contrary to the usual practice [37]. Because the refractive index of ZnSe ($\sim$2.40) is higher than that of BaF_2 ($\sim$1.46), ZnSe windows will generate higher amplitude interference fringes (Frame b). These are perfectly recovered in the calculated spectrum (26.3 μm ($\delta = 0.2\,\mu m$) sample thickness). As for the BaF_2 situation, the HDO bands appear in the experimental spectrum and not in the calculated one. Frame (c) shows the difference between cal-

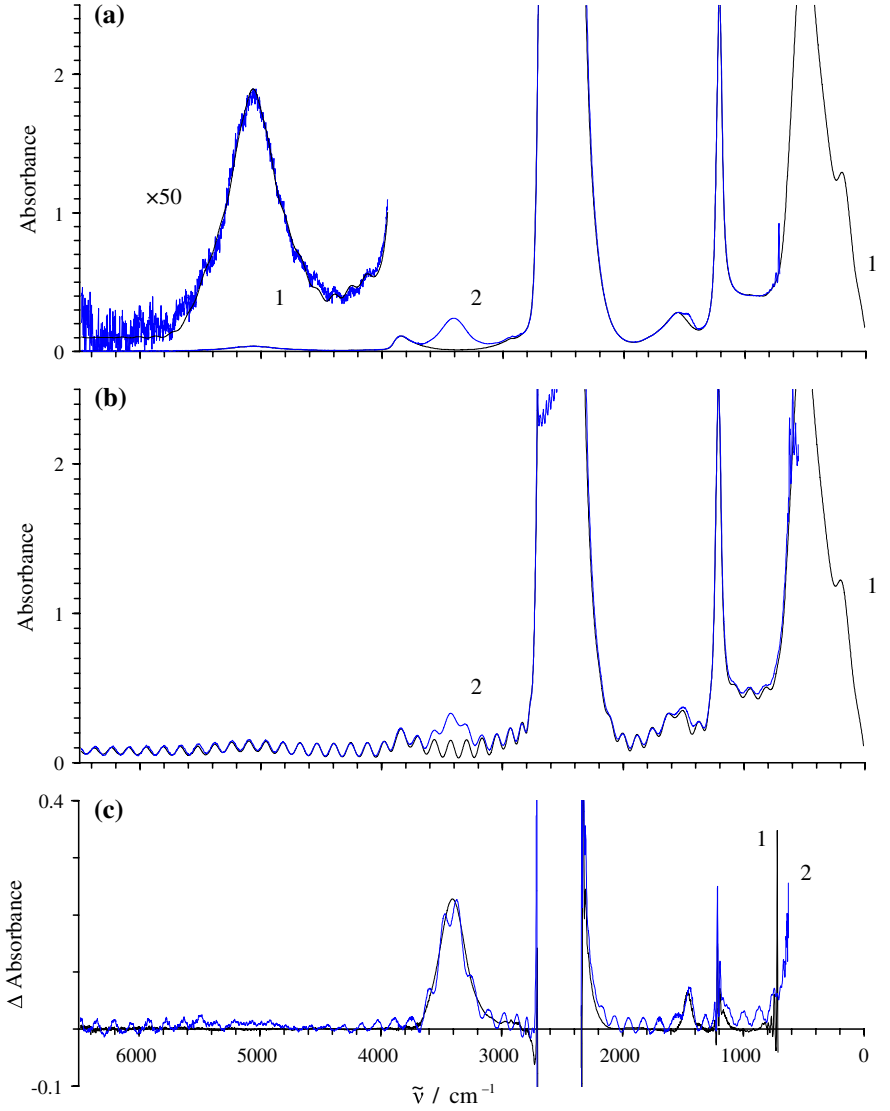

Fig. 10 Comparison between calculated (*1, black*) and experimental (*2, blue*) spectra of liquid D_2O between two windows: **a** BaF_2 with a pathlength of 27.4 μm; **b** ZnSe with a pathlength of 26.3 μm. Frame **c** is the difference between calculated and experimental spectra of D_2O between the two BaF_2 windows (*1, black*) and ZnSe ones (*2, blue*). (Color figure online)

culated and experimental spectra for the two cases. Except in the strong absorption regions were there is a blackout, the two spectra are almost coincident with a small sinusoidal remain in the spectrum (2) that originates from the ZnSe cell. The two HDO bands (∼3,400 and ∼14,700 cm^{-1}) are exactly matched. These results are a clear indication of the validity of the equations developed for thin IR window cells.

5 Conclusions

The interference fringes observed in transmission measurements of thin sample are difficult to quantify exactly which gives low accuracy of intensity measurements. The new equations that take into account the cell window material evaluate the effect of the multiple reflections encountered in transmission measurements. The new sets of equations give better results than those presently available.

To circumscribe the cell parallel window problems some authors proposed wedge shaped transmission cells [23]. Although these have some advantages they are not without difficulties. The spectra may show base line distortions and drifts. However, the new analytical equations given here tackle the problem effectively as the examples provided illustrate. Moreover, these equations deal with the problems of boxcar cells whose windows are not perfectly parallel or have minute surface imperfections.

The validity and usefulness of the equations presented here will take their full meaning in the measurements of pure liquid samples because these are obtained in a few micrometer thin cells that generate fringes. For liquid water for which the set of equations was developed they are essential. For pure liquids used as standards, the proposed equations will give better optical properties. These equations should be a valuable asset for all spectroscopists working with these liquids since the use of transmission cells with different pathlength [29–31] may not eliminate the error generated by the multiple internal reflections. The alternative way that we propose here is to compare, once the optical properties settled, the experimental results with those obtained from calculations. This is actually the way to obtain the best optical properties of pure liquids. For pure liquid light and heavy water, for which this mathematical incursion was made, these calculations will be used in a forthcoming paper that will give their newly calculated optical properties.

Acknowledgements This work was supported in part by a grant from the Natural Sciences and Engineering Research of Canada (NSERC).

6 Appendix A. Integration of the transmission equation over the sample thickness variation

The problem is to obtain an analytical form for integration of the approximation Eq. 38 that gives the transmission.

6.1 Development to the 2nd order in Q

Developing explicitly the series in Eq. (38) to the 2nd order in Q and integrating over sample thickness $\ell_1 \pm \delta$ gives:

$$\frac{1}{2\delta}\int_{\ell_1-\delta}^{\ell_1+\delta} \mathrm{T}\,\mathrm{d}\ell_1 \approx \left(1-\mathrm{r}_\mathrm{s}^2\right)^2 \left\|1-\mathrm{r}_2^{*2}\right\|^2 \mathrm{e}^{-(\alpha_1+\alpha_2+\alpha_3)} \times \left[\begin{array}{l} 1+\left(\mathrm{r}_{2R}^2+\mathrm{r}_{2I}^2\right)^2\mathrm{e}^{-2\alpha_1}+\left(\mathrm{r}_{2R}^2+\mathrm{r}_{2I}^2\right)^4\mathrm{e}^{-4\alpha_1} \\ \quad +\frac{1}{\delta}\mathrm{e}^{-\alpha_1}\left[1-2\left(\mathrm{r}_{2R}^2+\mathrm{r}_{2I}^2\right)^2\mathrm{e}^{-2\alpha_1}\right] \\ \quad \times\left\{\left(\mathrm{r}_{2R}^2-\mathrm{r}_{2I}^2\right)\int_{\ell_1-\delta}^{\ell_1+\delta}\cos\left(2\omega\mathrm{T}_1\right)\mathrm{d}\ell\right. \\ \qquad \left.+2\mathrm{r}_{2I}\mathrm{r}_{2R}\int_{\ell_1-\delta}^{\ell_1+\delta}\sin\left(2\omega\mathrm{T}_1\right)\mathrm{d}\ell\right\} \\ +\frac{1}{\delta}\mathrm{e}^{-2\alpha_1}\left\{\left[\left(\mathrm{r}_{2R}^2-\mathrm{r}_{2I}^2\right)^2-4\mathrm{r}_{2I}^2\mathrm{r}_{2R}^2\right]\int_{\ell_1-\delta}^{\ell_1+\delta}\cos\left(4\omega\mathrm{T}_1\right)\mathrm{d}\ell\right. \\ \qquad \left.+4\mathrm{r}_{2I}\mathrm{r}_{2R}\left(\mathrm{r}_{2R}^2-\mathrm{r}_{2I}^2\right)\int_{\ell_1-\delta}^{\ell_1+\delta}\sin\left(4\omega\mathrm{T}_1\right)\mathrm{d}\ell\right\} \end{array}\right] \tag{A1}$$

That is, after performing the integrations:

$$\frac{1}{2\delta}\int_{\ell_1-\delta}^{\ell_1+\delta} \mathrm{T}\,\mathrm{d}\ell_1 \approx \left(1-\mathrm{r}_\mathrm{s}^2\right)^2 \left\|1-\mathrm{r}_2^{*2}\right\|^2 \mathrm{e}^{-(\alpha_1+\alpha_2+\alpha_3)} \times \left[\begin{array}{l} 1+\left(\mathrm{r}_{2R}^2+\mathrm{r}_{2I}^2\right)^2\mathrm{e}^{-2\alpha_1}+\left(\mathrm{r}_{2R}^2+\mathrm{r}_{2I}^2\right)^4\mathrm{e}^{-4\alpha_1} \\ +\frac{\sin(400\pi\tilde{\nu}n_1\delta)}{200\pi\tilde{\nu}n_1\delta}\mathrm{e}^{-\alpha_1}\left[1-2\left(\mathrm{r}_{2R}^2+\mathrm{r}_{2I}^2\right)^2\mathrm{e}^{-2\alpha_1}\right] \\ \quad \times\left\{\left(\mathrm{r}_{2R}^2-\mathrm{r}_{2I}^2\right)\cos\left(2\omega\mathrm{T}_1\right)+2\mathrm{r}_{2I}\mathrm{r}_{2R}\sin\left(2\omega\mathrm{T}_1\right)\right\} \\ +\frac{\sin(800\pi\tilde{\nu}n_1\delta)}{400\pi\tilde{\nu}n_1\delta}\mathrm{e}^{-2\alpha_1}\left\{\left[\left(\mathrm{r}_{2R}^2-\mathrm{r}_{2I}^2\right)^2-4\mathrm{r}_{2I}^2\mathrm{r}_{2R}^2\right]\right. \\ \quad \left.\times\cos\left(4\omega\mathrm{T}_1\right)+4\mathrm{r}_{2I}\mathrm{r}_{2R}\left(\mathrm{r}_{2R}^2-\mathrm{r}_{2I}^2\right)\sin\left(4\omega\mathrm{T}_1\right)\right\} \end{array}\right] \tag{A2}$$

Equation (A2) indicates that the oscillations governed by the period (T_1) for light passing through the entire sample are modulated by the shorter oscillation period related to the sample thickness variation (δ). The modulation follows a damping that varies with frequency according to the form $\sin(\mathrm{X}\nu)/\mathrm{X}\nu$, where X is a quantity that relates to harmonics obtained from the development in Q.

In the limiting case of $\delta = 0$, Eq. (A2) should give the same result as Eqs. (26) and (32). However, this verification is not easy because Eq. (A2) was obtained by using an approximation of Eqs. (26) and (32).

6.2 Limit evaluation of Eq. (A2) at null frequency

At very low frequency, the terms of the form sin(2x)/x in Eq. (A2) can be replaced by a factor of 2 which is its limiting value for $\mathrm{x} \to 0$. This gives:

$$\frac{1}{2\delta}\int_{\ell_1-\delta}^{\ell_1+\delta} \mathrm{Td}\ell_1 \approx \left(1-\mathrm{r_s^2}\right)^2 \left\|1-\mathrm{r_2^{*2}}\right\|^2 \left[\begin{array}{l} 1+\left(\mathrm{r_{2R}^2}+\mathrm{r_{2I}^2}\right)^2+\left(\mathrm{r_{2R}^2}+\mathrm{r_{2I}^2}\right)^4 \\ \quad +2\left[1-2\left(\mathrm{r_{2R}^2}+\mathrm{r_{2I}^2}\right)^2\right]\left(\mathrm{r_{2R}^2}-\mathrm{r_{2I}^2}\right) \\ \quad +2\left[\left(\mathrm{r_{2R}^2}-\mathrm{r_{2I}^2}\right)^2 -4\mathrm{r_{2I}^2 r_{2R}^2}\right] \end{array}\right] \tag{A3}$$

That can be further reduced to:

$$\frac{1}{2\delta}\int_{\ell_1-\delta}^{\ell_1+\delta} \mathrm{Td}\ell_1 \approx \left(1-\mathrm{r_s^2}\right)^2 \left\|1-\mathrm{r_2^{*2}}\right\|^2 \left[1+2\mathrm{r_{2R}^2}+3\mathrm{r_{2R}^4}-4\mathrm{r_{2R}^6}+\mathrm{r_{2R}^8}\right] \tag{A4}$$

For $\nu = 0$, (i.e.: $\mathrm{r}_{2I} = 0$) the rightmost term in Eq. (A4) is different from that obtained directly with Eqs. (26) and (32) because it diverges above the 4th order in r_{2R}. Therefore, approximation by Eq. (A2) is not sufficient for even relatively low values of r_{2R}. Consequently a higher order is required for this evaluation.

6.3 Integration over sample thickness variations: 3rd order approximation

Developing Eq. (38) in series to the 3rd order in Q and integrating one gets:

$$\begin{aligned} \frac{1}{2\delta}\int_{\ell_1-\delta}^{\ell_1+\delta} \mathrm{Td}\ell_1 \approx{}& \left(1-\mathrm{r_s^2}\right)^2 \left\|1-\mathrm{r_2^{*2}}\right\|^2 \mathrm{e}^{-(\alpha_1+\alpha_2+\alpha_3)} \\ &\times \left[\begin{array}{l} 1+\left(\mathrm{r_{2R}^2}+\mathrm{r_{2I}^2}\right)^2\mathrm{e}^{-2\alpha_1}-5\left(\mathrm{r_{2R}^2}+\mathrm{r_{2I}^2}\right)^4\mathrm{e}^{-4\alpha_1}-\left(\mathrm{r_{2R}^2}+\mathrm{r_{2I}^2}\right)^6\mathrm{e}^{-6\alpha_1} \\ +\frac{\sin(400\pi\tilde{\nu}n_1\delta)}{200\pi\tilde{\nu}n_1\delta}\mathrm{e}^{-\alpha_1}\left[1+\left(\mathrm{r_{2R}^2}+\mathrm{r_{2I}^2}\right)^2\mathrm{e}^{-2\alpha_1}+3\left(\mathrm{r_{2R}^2}+\mathrm{r_{2I}^2}\right)^4\mathrm{e}^{-4\alpha_1}\right] \\ \quad \times\left[\begin{array}{l}\left(\mathrm{r_{2R}^2}-\mathrm{r_{2I}^2}\right)\cos(2\omega\mathrm{T}_1) \\ +2\mathrm{r_{2I}r_{2R}}\sin(2\omega\mathrm{T}_1)\end{array}\right] \\ +\frac{\sin(800\pi\tilde{\nu}n_1\delta)}{400\pi\tilde{\nu}n_1\delta}\mathrm{e}^{-2\alpha_1}\left[1-3\left(\mathrm{r_{2R}^2}+\mathrm{r_{2I}^2}\right)^2\mathrm{e}^{-2\alpha_1}\right] \\ \quad \times\left\{\begin{array}{l}\left[\left(\mathrm{r_{2R}^2}-\mathrm{r_{2I}^2}\right)^2-4\mathrm{r_{2I}^2r_{2R}^2}\right]\cos(4\omega\mathrm{T}_1) \\ +4\mathrm{r_{2I}r_{2R}}\left(\mathrm{r_{2R}^2}-\mathrm{r_{2I}^2}\right)\ \sin(4\omega\mathrm{T}_1)\end{array}\right\} \\ +\frac{\sin(1200\pi\tilde{\nu}n_1\delta)}{600\pi\tilde{\nu}n_1\delta}\mathrm{e}^{-3\alpha_1}\left\{\begin{array}{l}\left(\mathrm{r_{2R}^2}-\mathrm{r_{2I}^2}\right)\left[\left(\mathrm{r_{2R}^2}-\mathrm{r_{2I}^2}\right)^2-12\mathrm{r_{2I}^2r_{2R}^2}\right] \\ \quad \times\cos(6\omega\mathrm{T}_1) \\ +2\mathrm{r_{2I}r_{2R}}\left[3\left(\mathrm{r_{2R}^2}-\mathrm{r_{2I}^2}\right)^2-4\mathrm{r_{2I}^2r_{2R}^2}\right] \\ \quad \sin(6\omega\mathrm{T}_1)\end{array}\right\} \end{array}\right] \end{aligned} \tag{A5}$$

This is similar to Eq. (A2) obtained with a 2nd order approximation in Q but with supplementary trigonometric terms in $(6\omega\mathrm{T}_1)$. Terms in $\mathrm{e}^{-p\alpha_1}$ are identical in Eqs. (A5) and (A2) for $p = 0$, 1, and 2. This is due to the common part from the 2nd order in Q. In Eq. (A5), the coefficient of each term in $\mathrm{e}^{-p\alpha_1}$ with $p > 3$ will be modified

when using higher orders in Q and therefore are not exact. At null frequency, Eq. (A5) becomes:

$$\frac{1}{2\delta}\int_{\ell_1-\delta}^{\ell_1+\delta} \mathrm{Td}\ell_1 \approx \left(1-\mathrm{r_s^2}\right)^2 \left\|1-\mathrm{r_2^{*2}}\right\|^2 \mathrm{e}^{-(\alpha_1+\alpha_2+\alpha_3)} \times \left[1+2\mathrm{r}_{2R}^2\mathrm{e}^{-\alpha_1}+3\mathrm{r}_{2R}^4\mathrm{e}^{-2\alpha_1}+6\mathrm{r}_{2R}^6\mathrm{e}^{-3\alpha_1}-11\mathrm{r}_{2R}^8\mathrm{e}^{-4\alpha_1} +6\mathrm{r}_{2R}^{10}\mathrm{e}^{-5\alpha_1}-\mathrm{r}_{2R}^{12}\mathrm{e}^{-6\alpha_1}\right] \tag{A6}$$

This indicates that even the 3rd order used for the approximation in Eq. (38) is insufficient at null frequency for reflection ratio r_{2R} above 0.5. This is the case for water since its refractive index is above 3 from 0 to 5 cm^{-1} giving reflection coefficient above 0.5 with BaF_2 and ZnSe windows. This difficulty is surmounted by increasing the order of approximation in Eq. (38).

6.4 Integration over sample thickness variations: 4th order approximation

Developing $1/(1+Q)$ in series to the 4th order in Q one gets:

$$\begin{aligned}
&1-Q\left(l_1\right)+Q^2\left(l_1\right)-Q^3\left(l_1\right)+Q^4\left(l_1\right)\cdots \\
&= \left\{\begin{array}{l}
1+\left(\mathrm{r}_{2R}^2+\mathrm{r}_{2I}^2\right)^2\mathrm{e}^{-2\alpha_1}+\left(\mathrm{r}_{2R}^2+\mathrm{r}_{2I}^2\right)^4\mathrm{e}^{-4\alpha_1} \\
\quad +11\left(\mathrm{r}_{2R}^2+\mathrm{r}_{2I}^2\right)^6\mathrm{e}^{-6\alpha_1}+\left(\mathrm{r}_{2R}^2+\mathrm{r}_{2I}^2\right)^8\mathrm{e}^{-8\alpha_1} \\
+2\mathrm{e}^{-\alpha_1}\left[1+\left(\mathrm{r}_{2R}^2+\mathrm{r}_{2I}^2\right)^2\mathrm{e}^{-2\alpha_1}-9\left(\mathrm{r}_{2R}^2+\mathrm{r}_{2I}^2\right)^4\mathrm{e}^{-4\alpha_1}\right. \\
\qquad \left.-4\left(\mathrm{r}_{2R}^2+\mathrm{r}_{2I}^2\right)^6\mathrm{e}^{-6\alpha_1}\right] \\
\quad \times\left[\left(\mathrm{r}_{2R}^2-\mathrm{r}_{2I}^2\right)\cos\left(2\omega\mathrm{T}_1\right)+2\mathrm{r}_{2I}\mathrm{r}_{2R}\sin\left(2\omega\mathrm{T}_1\right)\right] \\
+2\mathrm{e}^{-2\alpha_1}\left[1+\left(\mathrm{r}_{2R}^2+\mathrm{r}_{2I}^2\right)^2\mathrm{e}^{-2\alpha_1}+6\left(\mathrm{r}_{2R}^2+\mathrm{r}_{2I}^2\right)^4\mathrm{e}^{-4\alpha_1}\right] \\
\quad \times\left[\left(\mathrm{r}_{2R}^2-\mathrm{r}_{2I}^2\right)^2-4\mathrm{r}_{2I}^2\mathrm{r}_{2R}^2\right]\cos\left(4\omega\mathrm{T}_1\right) \\
\quad +4\mathrm{r}_{2I}\mathrm{r}_{2R}\left(\mathrm{r}_{2R}^2-\mathrm{r}_{2I}^2\right)\sin\left(4\omega\mathrm{T}_1\right) \\
+2\mathrm{e}^{-3\alpha_1}\left[1-4\left(\mathrm{r}_{2R}^2+\mathrm{r}_{2I}^2\right)^2\mathrm{e}^{-2\alpha_1}\right]\left(\mathrm{r}_{2R}^2-\mathrm{r}_{2I}^2\right) \\
\quad \times\left[\left(\mathrm{r}_{2R}^2-\mathrm{r}_{2I}^2\right)^2-12\mathrm{r}_{2I}^2\mathrm{r}_{2R}^2\right]\cos\left(6\omega\mathrm{T}_1\right)+2\mathrm{r}_{2I}\mathrm{r}_{2R} \\
\quad \times\left[3\left(\mathrm{r}_{2R}^2-\mathrm{r}_{2I}^2\right)^2-4\mathrm{r}_{2I}^2\mathrm{r}_{2R}^2\right]\sin\left(6\omega\mathrm{T}_1\right) \\
+2\mathrm{e}^{-4\alpha_1}\left[\left(\mathrm{r}_{2R}^2-\mathrm{r}_{2I}^2\right)^4+16\mathrm{r}_{2I}^4\mathrm{r}_{2R}^4-24\left(\mathrm{r}_{2R}^2-\mathrm{r}_{2I}^2\right)^2\mathrm{r}_{2I}^2\mathrm{r}_{2R}^2\right] \\
\quad \times\cos\left(8\omega\mathrm{T}_1\right)+8\left(\mathrm{r}_{2R}^2-\mathrm{r}_{2I}^2\right)\mathrm{r}_{2I}\mathrm{r}_{2R}\left[\left(\mathrm{r}_{2R}^2-\mathrm{r}_{2I}^2\right)^2-4\mathrm{r}_{2I}^2\mathrm{r}_{2R}^2\right] \\
\quad \times\sin\left(8\omega\mathrm{T}_1\right)
\end{array}\right.
\end{aligned} \tag{A7}$$

At the approximation order used in Q (4th), the coefficient of each term in $e^{-p\alpha_1}$ with $p < 5$ are the right ones. Terms with $p > 4$ will be modified when using higher orders in Q and therefore are not exact.

At this stage, one can distinguish two kinds of approximation parameters: the first one is simply the order of the approximation in Q; the second one is the approximation in the harmonics level of the result. Approximation at the pth order in Q will produce terms up to the pth harmonics in modulation frequency of the oscillation amplitudes. However, the coefficient relative to each of the harmonics obtained by this way are not the exact ones because further terms will be added to them by increasing the approximation order in Q. As a result, approximation will remain poor at very low frequency, due to the inaccuracy, for instance, of the 0^{th} harmonics coefficient.

Fortunately, Eq. (A7) permits drawing the picture of the results from a higher order approximation in Q relative to the lower harmonics terms in $\cos(2p\omega T_1)$ and $\sin(2p\omega T_1)$. From Eq. (A7) we deduce the approximation of Eq. (32) at the fourth harmonics in modulating function ($p = 4$, that is: $8\omega T_1$):

$$
\begin{aligned}
&1 - Q(l_1) + Q^2(l_1) - Q^3(l_1) + Q^4(l_1) \cdots \\
&= \left\{ \begin{array}{l}
\displaystyle\sum_{p=0}^{\infty} \left[\left(r_{2R}^2 + r_{2I}^2\right)^2 e^{-2\alpha_1} \right]^p \\
+2e^{-\alpha_1} \displaystyle\sum_{p=0}^{\infty} \left[\left(r_{2R}^2 + r_{2I}^2\right)^2 e^{-2\alpha_1} \right]^p \\
\quad \times \left[\left(r_{2R}^2 - r_{2I}^2\right) \cos(2\omega T_1) + 2 r_{2I} r_{2R} \sin(2\omega T_1) \right] \\
+2e^{-2\alpha_1} \displaystyle\sum_{p=0}^{\infty} \left[\left(r_{2R}^2 + r_{2I}^2\right)^2 e^{-2\alpha_1} \right]^p \left\{ \left[\left(r_{2R}^2 - r_{2I}^2\right)^2 - 4 r_{2I}^2 r_{2R}^2 \right] \right. \\
\quad \left. \times \cos(4\omega T_1) + 4 r_{2I} r_{2R} \left(r_{2R}^2 - r_{2I}^2\right) \sin(4\omega T_1) \right\} \\
+2e^{-3\alpha_1} \displaystyle\sum_{p=0}^{\infty} \left[\left(r_{2R}^2 + r_{2I}^2\right)^2 e^{-2\alpha_1} \right]^p \left\{ \left(r_{2R}^2 - r_{2I}^2\right) \right. \\
\quad \times \left[\left(r_{2R}^2 - r_{2I}^2\right)^2 - 12 r_{2I}^2 r_{2R}^2 \right] \cos(6\omega T_1) \\
\quad \left. + 2 r_{2I} r_{2R} \left[3 \left(r_{2R}^2 - r_{2I}^2\right)^2 - 4 r_{2I}^2 r_{2R}^2 \right] \sin(6\omega T_1) \right\} \\
+2e^{-4\alpha_1} \displaystyle\sum_{p=0}^{\infty} \left[\left(r_{2R}^2 + r_{2I}^2\right)^2 e^{-2\alpha_1} \right]^p \\
\quad \times \left\{ \begin{array}{l}
\left[\left(r_{2R}^2 - r_{2I}^2\right)^4 + 16 r_{2I}^4 r_{2R}^4 - 24 \left(r_{2R}^2 - r_{2I}^2\right)^2 r_{2I}^2 r_{2R}^2 \right] \cos(8\omega T_1) \\
+8 \left(r_{2R}^2 - r_{2I}^2\right) r_{2I} r_{2R} \left[\left(r_{2R}^2 - r_{2I}^2\right)^2 - 4 r_{2I}^2 r_{2R}^2 \right] \sin(8\omega T_1)
\end{array} \right\} \\
\quad + f\left(\cos(2p\omega T_1), \sin(2p\omega T_1), p > 4\right)
\end{array} \right.
\end{aligned}
\tag{A8}
$$

This is simplified to:

$$1-Q\left(l_1\right)+Q^2\left(l_1\right)-Q^3\left(l_1\right)+Q^4\left(l_1\right)\cdots=\frac{1}{1-\left(\mathrm{r}_{2R}^2+\mathrm{r}_{2I}^2\right)^2\mathrm{e}^{-2\alpha_1}}$$

$$\times\left\{\begin{array}{l}1\\ +2\mathrm{e}^{-\alpha_1}\left[\left(\mathrm{r}_{2R}^2-\mathrm{r}_{2I}^2\right)\cos\left(2\omega\mathrm{T}_1\right)+2\mathrm{r}_{2I}\mathrm{r}_{2R}\sin\left(2\omega\mathrm{T}_1\right)\right]\\ +2\mathrm{e}^{-2\alpha_1}\left\{\left[\left(\mathrm{r}_{2R}^2-\mathrm{r}_{2I}^2\right)^2-4\mathrm{r}_{2I}^2\mathrm{r}_{2R}^2\right]\cos\left(4\omega\mathrm{T}_1\right)\right.\\ \qquad\left.+\,4\mathrm{r}_{2I}\mathrm{r}_{2R}\left(\mathrm{r}_{2R}^2-\mathrm{r}_{2I}^2\right)\sin\left(4\omega\mathrm{T}_1\right)\right\}\\ +2\mathrm{e}^{-3\alpha_1}\left\{\left(\mathrm{r}_{2R}^2-\mathrm{r}_{2I}^2\right)\left[\left(\mathrm{r}_{2R}^2-\mathrm{r}_{2I}^2\right)^2-12\mathrm{r}_{2I}^2\mathrm{r}_{2R}^2\right]\cos\left(6\omega\mathrm{T}_1\right)\right.\\ \qquad\left.+\,2\mathrm{r}_{2I}\mathrm{r}_{2R}\left[3\left(\mathrm{r}_{2R}^2-\mathrm{r}_{2I}^2\right)^2-4\mathrm{r}_{2I}^2\mathrm{r}_{2R}^2\right]\sin\left(6\omega\mathrm{T}_1\right)\right\}\\ +2\mathrm{e}^{-4\alpha_1}\left\{\begin{array}{l}\left[\left(\mathrm{r}_{2R}^2-\mathrm{r}_{2I}^2\right)^4+16\mathrm{r}_{2I}^4\mathrm{r}_{2R}^4-24\left(\mathrm{r}_{2R}^2-\mathrm{r}_{2I}^2\right)^2\mathrm{r}_{2I}^2\mathrm{r}_{2R}^2\right]\cos\left(8\omega\mathrm{T}_1\right)\\ +8\left(\mathrm{r}_{2R}^2-\mathrm{r}_{2I}^2\right)\mathrm{r}_{2I}\mathrm{r}_{2R}\left[\left(\mathrm{r}_{2R}^2-\mathrm{r}_{2I}^2\right)^2-4\mathrm{r}_{2I}^2\mathrm{r}_{2R}^2\right]\sin\left(8\omega\mathrm{T}_1\right)\end{array}\right\}\\ \quad+f\left(\cos\left(2p\omega\mathrm{T}_1\right),\sin\left(2p\omega\mathrm{T}_1\right),p>4\right)\end{array}\right. \tag{A9}$$

In this, the coefficients affecting higher periods of $p>4$ cannot be evaluated easily. Integration of Eq. (38) with Eq. (A9) on sample thickness $\lambda_1\pm\delta$ gives:

$$\frac{1}{2\delta}\int_{\ell_1-\delta}^{\ell_1+\delta}\mathrm{Td}\ell_1\approx\left(1-\mathrm{r}_{\mathrm{s}}^2\right)^2\left\|1-\mathrm{r}_2^{*2}\right\|^2\mathrm{e}^{-(\alpha_1+\alpha_2+\alpha_3)}\times\frac{1}{1-\left(\mathrm{r}_{2R}^2+\mathrm{r}_{2I}^2\right)^2\mathrm{e}^{-2\alpha_1}}$$

$$\times\left\{\begin{array}{l}1\\ +\frac{\sin(400\pi\tilde{\nu}n_1\delta)}{200\pi\tilde{\nu}n_1\delta}\mathrm{e}^{-\alpha_1}\left[\left(\mathrm{r}_{2R}^2-\mathrm{r}_{2I}^2\right)\cos\left(2\omega\mathrm{T}_1\right)+2\mathrm{r}_{2I}\mathrm{r}_{2R}\sin\left(2\omega\mathrm{T}_1\right)\right]\\ +\frac{\sin(800\pi\tilde{\nu}n_1\delta)}{400\pi\tilde{\nu}n_1\delta}\mathrm{e}^{-2\alpha_1}\left\{\left[\left(\mathrm{r}_{2R}^2-\mathrm{r}_{2I}^2\right)^2-4\mathrm{r}_{2I}^2\mathrm{r}_{2R}^2\right]\cos\left(4\omega\mathrm{T}_1\right)\right.\\ \qquad\left.+\,4\mathrm{r}_{2I}\mathrm{r}_{2R}\left(\mathrm{r}_{2R}^2-\mathrm{r}_{2I}^2\right)\sin\left(4\omega\mathrm{T}_1\right)\right\}\\ +\frac{\sin(1200\pi\tilde{\nu}n_1\delta)}{600\pi\tilde{\nu}n_1\delta}\mathrm{e}^{-3\alpha_1}\left(\mathrm{r}_{2R}^2-\mathrm{r}_{2I}^2\right)\left[\left(\mathrm{r}_{2R}^2-\mathrm{r}_{2I}^2\right)^2-12\mathrm{r}_{2I}^2\mathrm{r}_{2R}^2\right]\\ \quad\times\cos\left(6\omega\mathrm{T}_1\right)+2\mathrm{r}_{2I}\mathrm{r}_{2R}\left[3\left(\mathrm{r}_{2R}^2-\mathrm{r}_{2I}^2\right)^2-4\mathrm{r}_{2I}^2\mathrm{r}_{2R}^2\right]\sin\left(6\omega\mathrm{T}_1\right)\\ +\frac{\sin(1600\pi\tilde{\nu}n_1\delta)}{800\pi\tilde{\nu}n_1\delta}\mathrm{e}^{-4\alpha_1}\\ \quad\times\left\{\begin{array}{l}\left[\left(\mathrm{r}_{2R}^2-\mathrm{r}_{2I}^2\right)^4+16\mathrm{r}_{2I}^4\mathrm{r}_{2R}^4-24\left(\mathrm{r}_{2R}^2-\mathrm{r}_{2I}^2\right)^2\mathrm{r}_{2I}^2\mathrm{r}_{2R}^2\right]\cos\left(8\omega\mathrm{T}_1\right)\\ +8\left(\mathrm{r}_{2R}^2-\mathrm{r}_{2I}^2\right)\mathrm{r}_{2I}\mathrm{r}_{2R}\left[\left(\mathrm{r}_{2R}^2-\mathrm{r}_{2I}^2\right)^2-4\mathrm{r}_{2I}^2\mathrm{r}_{2R}^2\right]\sin\left(8\omega\mathrm{T}_1\right)\end{array}\right\}\\ \quad+f\left(\cos\left(2p\omega\mathrm{T}_1\right),\sin\left(2p\omega\mathrm{T}_1\right),p>4\right)\end{array}\right. \tag{A10}$$

A discussion on the order of the series development required to provide the desired accuracy is given in Appendix (B). In the following we give a simple way to obtain terms at higher harmonics from higher order approximation in Q in Eq. (38).

6.5 Integration over sample thickness variations: 5th harmonic approximation

Addition of the 5th order approximation to Eq. (A10) requires the term coefficients with period $10\omega\mathrm{T}_1$. These necessarily come from $\sin^p(s)\times\cos^q(s)$ terms having $(p+q)=5$. There are six possibilities that need to be transformed into $\sin(\mathrm{u}s)$ and $\cos(\mathrm{u}s)$ terms with u = 1–5:

$$\begin{cases} \cos^5(s) = \frac{5}{8}\cos(s) + \frac{5}{16}\cos(3q) + \frac{1}{16}\cos(5s) \\ \cos^4(s)\sin(s) = \frac{1}{8}\sin(s) + \frac{3}{16}\sin(3s) + \frac{1}{16}\sin(5s) \\ \cos^3(s)\sin^2(s) = \frac{1}{8}\cos(s) - \frac{1}{16}\cos(3s) - \frac{1}{16}\cos(5s) \\ \cos^2(s)\sin^3(s) = \frac{1}{8}\sin(s) + \frac{1}{16}\sin(3s) - \frac{1}{16}\sin(5s) \\ \cos(s)\sin^4(s) = \frac{1}{8}\cos(s) - \frac{3}{16}\cos(3s) + \frac{1}{16}\cos(5s) \\ \sin^5(s) = \frac{5}{8}\sin(s) - \frac{5}{16}\sin(3s) + \frac{1}{16}\sin(5s) \end{cases} \tag{A11}$$

Furthermore, defining from Eq. (37): $Q = a\cos(2\omega T_1) - b\sin(2\omega T_1) + c$, ($a$, b, and c are three coefficients that do not depend on T_1) the $\sin^p \times \cos^q$ terms with $(p+q) = 5$ will come from the following combinations from $(-Q)^5$: a^5, $5a^4b$, $-10a^3b^2$, $10a^2b^3$, $5ab^4$, and b^5. Every term containing c will be of a lower power $(p+q) < 5$. From Eq. (A11), terms in $\cos(5s)$ will come from a^5, $-10a^3b^2$, and $5ab^4$, while those in $\sin(5s)$ from $5a^4b$, $-10a^2b^3$, and b^5. The multiplier of each $\cos(5s)$ and $\sin(5s)$ term is 1/16 in Eq. (A11). Hence one obtains:

$$\begin{cases} a\left[a^4 - 10a^2b^2 + 5b^4\right]\cos(10\omega T_1) \\ +b\left[5a^4 - 10a^2b^2 + b^4\right]\sin(10\omega T_1) \end{cases} \tag{A12}$$

Replacing a and b by their value taken from Eq. (37), taking care of the respective sign of $\cos(5s)$ and $\sin(5s)$ in Eq. (A11), one gets:

$$e^{-5\alpha_1}\begin{cases} \frac{1}{16}2\left(r_{2R}^2 - r_{2I}^2\right)\left[16\left(r_{2R}^2 - r_{2I}^2\right)^4 - 10\times 4\left(r_{2R}^2 - r_{2I}^2\right)^2\right. \\ \quad \left.\times 16r_{2I}^2 r_{2R}^2 + 5\times 256 r_{2I}^4 r_{2R}^4\right]\cos(10\omega T_1) \\ +\frac{1}{16}4r_{2I}r_{2R}\left[5\times 16\left(r_{2R}^2 - r_{2I}^2\right)^4 - 10\times 4\left(r_{2R}^2 - r_{2I}^2\right)^2\right. \\ \quad \left.\times 16r_{2I}^2 r_{2R}^2 + 256 r_{2I}^4 r_{2R}^4\right]\sin(10\omega T_1) \end{cases} \tag{A13}$$

This simplifies into:

$$2e^{-5\alpha_1}\begin{cases} \left(r_{2R}^2 - r_{2I}^2\right)\left[\left(r_{2R}^2 - r_{2I}^2\right)^4 - 40\left(r_{2R}^2 - r_{2I}^2\right)^2 r_{2I}^2 r_{2R}^2 + 80 r_{2I}^4 r_{2R}^4\right] \\ \quad \times\cos(10\omega T_1) \\ +2r_{2I}r_{2R}\left[5\left(r_{2R}^2 - r_{2I}^2\right)^4 - 40\left(r_{2R}^2 - r_{2I}^2\right)^2 r_{2I}^2 r_{2R}^2 + 16 r_{2I}^4 r_{2R}^4\right] \\ \quad \times\sin(10\omega T_1) \end{cases} \tag{A14}$$

The term in this is added into Eq. (A9). The integration of term given by Eq. (A14) performed similarly to that for lower harmonics gives

$$+\frac{\sin(2000\pi\tilde{\nu}n_1\delta)}{1000\pi\tilde{\nu}n_1\delta}e^{-5\alpha_1}\begin{cases} \left(r_{2R}^2 - r_{2I}^2\right)\left[\left(r_{2R}^2 - r_{2I}^2\right)^4 - 40\left(r_{2R}^2 - r_{2I}^2\right)^2\right. \\ \quad \left.\times r_{2I}^2 r_{2R}^2 + 80 r_{2I}^4 r_{2R}^4\right]\cos(10\omega T_1) \\ +2r_{2I}r_{2R}\left[5\left(r_{2R}^2 - r_{2I}^2\right)^4 - 40\left(r_{2R}^2 - r_{2I}^2\right)^2\right. \\ \quad \left.\times r_{2I}^2 r_{2R}^2 + 16 r_{2I}^4 r_{2R}^4\right]\sin(10\omega T_1) \end{cases} \tag{A15}$$

The above term is added to Eq. (A10) to give the result at one higher harmonic. This calculation technique can be used to increase the harmonic level in the approximation up to the desired accuracy. See Appendix B for details.

6.6 Integration over sample thickness variations: 6th harmonic approximation

Similarily to the addition of the 5th harmonics, the addition of the 6th order harmonics only requires the term coefficients with period $12\omega T_1$. These necessarily come from $\sin^p(s) \times \cos^q(s)$ terms having $(p+q) = 6$. There are seven possibilities that need to be transformed into $\sin(us)$ and $\cos(us)$ terms with u varying from 1 to 6:

$$\begin{cases} \cos^6(s) = \frac{5}{16} + \frac{15}{32}\cos(2s) + \frac{3}{16}\cos(4s) + \frac{1}{32}\cos(6s) \\ \cos^5(s)\sin(s) = \frac{5}{32}\sin(2s) + \frac{1}{8}\sin(4s) + \frac{1}{32}\sin(6s) \\ \cos^4(s)\sin^2(s) = \frac{1}{16} + \frac{1}{32}\cos(2s) - \frac{1}{16}\cos(4s) - \frac{1}{32}\cos(6s) \\ \cos^3(s)\sin^3(s) = \frac{3}{32}\sin(2s) - \frac{1}{32}\sin(6s) \\ \cos^2(s)\sin^4(s) = \frac{1}{16} - \frac{1}{32}\cos(2s) - \frac{1}{16}\cos(4s) + \frac{1}{32}\cos(6s) \\ \cos(s)\sin^5(s) = \frac{5}{32}\sin(2s) - \frac{1}{8}\sin(4s) + \frac{1}{32}\sin(6s) \\ \sin^6(s) = \frac{5}{16} - \frac{15}{32}\cos(2s) + \frac{3}{16}\cos(4s) - \frac{1}{32}\cos(6s) \end{cases} \tag{A16}$$

Since $Q = -a\cos(2\omega T_1) - b\sin(2\omega T_1) + c$, the $\sin^p \times \cos^q$ terms with $(p+q) = 6$ will come from the following combination obtained from $(-Q)^6$ only: a^6, $6a^5b$, $15a^4b^2$, $20a^3b^3$, $15a^2b^4$, $6ab^5$, and b^6. According to Eq. (54), terms in $\cos(6s)$ will come from a^6, $-15a^4b^2$, $+15a^2b^4$, and $-b^6$, and those in $\sin(6s)$ from $6a^5b$, $-20a^3b^3$, and $+6ab^5$. The multiplier of each $\cos(6s)$ and $\sin(6s)$ term is 1/32 in Eq. (A16). Hence:

$$\begin{cases} \left[a^6 - 15a^4b^2 + 15a^2b^4 - b^6\right]\cos(12\omega T_1) \\ + \left[6a^5b - 20a^3b^3 + 6ab^5\right]\sin(12\omega T_1) \end{cases} \tag{A17}$$

Replacing a and b by their value taken from Eq. (37) into Eq. (A17) and rearranging, one gets:

$$2e^{-6\alpha_1} \begin{cases} \left[\left(r_{2R}^2 - r_{2I}^2\right)^6 - 60\left(r_{2R}^2 - r_{2I}^2\right)^4 r_{2I}^2 r_{2R}^2 \right. \\ \quad \left. + 240\left(r_{2R}^2 - r_{2I}^2\right)^2 r_{2I}^4 r_{2R}^4 - 64 r_{2I}^6 r_{2R}^6\right]\cos(12\omega T_1) \\ + \left[12\left(r_{2R}^2 - r_{2I}^2\right)^5 r_{2I} r_{2R} - 160\left(r_{2R}^2 - r_{2I}^2\right)^3 r_{2I}^3 r_{2R}^3 \right. \\ \quad \left. + 192\left(r_{2R}^2 - r_{2I}^2\right) r_{2I}^5 r_{2R}^5\right]\sin(12\omega T_1) \end{cases} \tag{A18}$$

This term is added into Eq. (A9) after adding that in Eq. (A14). The integration of term given by Eq. (56) performed similarly to lower harmonics gives

$$+\frac{\sin\left(2400\pi\tilde{\nu}n_1\delta\right)}{1200\pi\tilde{\nu}n_1\delta}$$
$$\times e^{-6\alpha_1}\left\{\begin{array}{l}\left[\left(r_{2R}^2-r_{2I}^2\right)^6-60\left(r_{2R}^2-r_{2I}^2\right)^4 r_{2I}^2 r_{2R}^2\right.\\ \left.\quad+240\left(r_{2R}^2-r_{2I}^2\right)^2 r_{2I}^4 r_{2R}^4-64 r_{2I}^6 r_{2R}^6\right]\cos\left(12\omega T_1\right)\\ +\left[12\left(r_{2R}^2-r_{2I}^2\right)^5 r_{2I} r_{2R}-160\left(r_{2R}^2-r_{2I}^2\right)^3 r_{2I}^3 r_{2R}^3\right.\\ \left.\quad+192\left(r_{2R}^2-r_{2I}^2\right) r_{2I}^5 r_{2R}^5\right]\sin\left(12\omega T_1\right)\end{array}\right. \tag{A19}$$

This term is added to Eq. (A10) along with that given by Eq. (A15) to give the evaluation of the transmission with one higher harmonic.

7 Appendix B. Discussion on the approximation accuracy

Let a be the accuracy level required for the transmission approximation. Let r be the reflection coefficient (real part) at the sample window interface. Interferences are generated by two reflections simultaneously (one on each face of the sample at the transparent windows) giving the reflection factor of r^2. Equation (A10) and others contain this term (for the real part of reflection only). Therefore, the approximation order n in r (from approximations in Q) should satisfy the relation $r^{2n} < a < 1$. This gives: $n \ln\left(r^2\right) < \ln(a) < 0$ and after rearrangement $n > \frac{\ln(a)}{\ln(r)}$. With this estimation, approximation to the 4th order in Q (in r^2) give an error less than 1% in the evaluation of the transmission for an r less than 0.5. Furthermore, Eq. (A10) already includes higher orders except for the terms oscillating with a period above $8\omega T_1$.

8 Appendix C. Validity of the approximation: $\frac{1}{2\delta}\int_{\ell-\delta}^{\ell+\delta} e^{-Kx}dx \approx e^{-K\ell}$

In Eq. (39), we neglected the influence of the sample thickness variation on the overall intensity in absorbance, simply taking:

$$\frac{1}{2\delta}\int_{\ell-\delta}^{\ell+\delta} e^{-Kx}dx \approx e^{-K\ell}, \tag{C1}$$

where K is the usual extinction coefficient (absorption coefficient in unit of m^{-1}). According to the properties of the exponential function, one gets:

$$\begin{aligned}\frac{1}{2\delta}\int_{\ell-\delta}^{\ell+\delta} e^{-Kx}dx &= \frac{1}{2\delta}\left[-\frac{1}{K}e^{-K(\ell+\delta)}-\left\{-\frac{1}{K}e^{-K(\ell-\delta)}\right\}\right]\\ &= \frac{1}{2K\delta}e^{-K\ell}\left(e^{+K\delta}-e^{-K\delta}\right)\end{aligned} \tag{C2}$$

Replacing the exponential by its series development at the 4th order:

$$\frac{1}{2\delta}\int_{\ell-\delta}^{\ell+\delta} e^{-Kx}dx \begin{cases} = \frac{1}{2K\delta}e^{-K\ell}\left[1 + K\delta + \frac{(K\delta)^2}{2} + \frac{(K\delta)^3}{6} \right. \\ \quad \left. + \cdots - \left(1 - K\delta + \frac{(K\delta)^2}{2} - \frac{(K\delta)^3}{6}\right)\right] \\ = \frac{1}{2K\delta}e^{-K\ell}\left[2K\delta + 2\frac{(K\delta)^3}{6}\right] \\ = e^{-K\ell}\left[1 + \frac{(K\delta)^2}{6}\right] \end{cases} \tag{C3}$$

The relative accuracy of the approximation $\frac{1}{2\delta}\int_{\ell-\delta}^{\ell+\delta} e^{-Kx}dx \approx e^{-K\ell}$ is therefore given by: $\frac{(K\delta)^2}{6}$. On the absorbance scale, it gives a different level of accuracy:

$$\begin{aligned} \log\left(\frac{1}{2\delta}\int_{\ell-\delta}^{\ell+\delta} e^{-Kx}dx\right) &= \log\left(e^{-K\ell}\left[1 + \frac{(K\delta)^2}{6}\right]\right) \\ &= \frac{-K\ell}{\ln(10)} + \log\left(1 + \frac{(K\delta)^2}{6}\right) \end{aligned} \tag{C4}$$

Hence, the relative error in intensity is transformed in an offset in absorbance (a decrease of the absorbance in accordance to what was observed for very thin samples). The decrease of absorbance only depends on the variation of the sample thickness. However, the relative absorbance error is strongly dependent on the sample thickness itself. This means that the relative error will be higher for thinner samples. This agrees with what was observed with very thin water samples (less than 6 μm). Further, the absorbance error could be put in the following form:

$$\log\left(1 + \frac{(K\delta)^2}{6}\right) = \frac{1}{\ln(10)}\left[\frac{(K\delta)^2}{6} - \frac{(K\delta)^4}{72} + \cdots\right] \tag{C5}$$

Application to the water spectrum: $K = 0.28\,\mu\text{m}^{-1}$ at $800\,\text{cm}^{-1}$ [9–11]; a thickness variation of $\delta = 0.4\,\mu\text{m}$ will give a small absorbance error of 1 mAU. However, a thickness variation of $\delta = 3.7\,\mu\text{m}$ will give an absorbance error of 78 mAU. This cannot be neglected.

In Eq. (39), the term $e^{-\alpha_1}$ in the first factor of the right member of this equation should be replaced by: $e^{-\alpha_1}\left[1 + \frac{1}{6}\left(\alpha_1\frac{\delta}{\ell_1}\right)^2\right]$. Every other places in the oscillating terms were $e^{-\alpha_1}$ appears could stay unchanged because it only slightly affects the oscillation amplitudes.

9 Appendix D. Effect of window thickness variation

Let d be the thickness of a window made of material with real refractive index n. The phase change for two passes through the material at wave frequency ν is:

$$\varphi_d^{\nu} = 2\pi\nu\frac{2dn}{c} \tag{D1}$$

where c is the speed of light. Let ν_0 be the frequency for which the phase change in φ_d^{ν} is 2π:

$$\nu_0 = \frac{c}{2dn} \tag{D2}$$

Let $\nu_m = \mathrm{m}\nu_0$ be a multiple of the resonant frequency ν_0. At this frequency, the phase change is $\varphi_d^{\nu_m} = m\varphi_d^{\nu_0}$. Let δ be an increase of thickness d for which the phase change $\varphi_{d+\delta}^{\nu_m}$ at frequency ν_m increases by π from that at thickness d, which is:

$$\varphi_{d+\delta}^{\nu_m} - \varphi_d^{\nu_m} = \pi, \tag{D3}$$

This gives:

$$4\pi m\nu_0\frac{\delta}{c}n = \pi \tag{D4}$$

Introducing Eq. (D2) into (D4) gives:

$$\delta = \frac{d}{2m} \tag{D5}$$

For example, interference fringes separated by $0.5\mathrm{cm}^{-1}$ (that comes from window thickness d and refractive index n) will disappear almost completely at $50\,\mathrm{cm}^{-1}$ ($m = 100$) with a window thickness variation superior than $\pm 0.5\%$ ($\delta/d = [2\times\mathrm{m}]^{-1}$).

The phase difference due to the thickness difference δ is:

$$\frac{\varphi_{d+\delta}^{\tilde{\nu}} - \varphi_d^{\tilde{\nu}}}{2\pi} = 200n\tilde{\nu}\delta, \tag{D6}$$

Introducing Eq. (D5) into (D6) gives:

$$\frac{\varphi_{d+\delta}^{\tilde{\nu}} - \varphi_d^{\tilde{\nu}}}{2\pi} = 100n\frac{d}{m}\tilde{\nu}, \tag{D7}$$

Hence, for a given value of $\delta(= d/m)$ the phase difference increases with frequency. The frequency for which the phase difference is exactly 2π is: $\tilde{\nu} = \frac{1}{200n\delta}$. Therefore, integration over the thickness variation will not cover an exact number of period at all frequencies so that a beat in the oscillations will be observed as in Fig. 8.

However, oscillation amplitude will decrease with increasing frequency. For instance, for $\delta = 0.01$ mm (0.3% of 3 mm windows) gives 500 cm^{-1} for the 1st extinction. This cyclic damping could be used to obtain the sample thickness variation.

References

1. J.-J. Max, C. Chapados, J. Chem. Phys. **116**, 4626 (2002)
2. P. Larouche, J.-J. Max, C. Chapados, J. Chem. Phys. **129**, 064503 (2008)
3. J.-J. Max, V. Gessinger, C. van Driessche, P. Larouche, C. Chapados, J. Chem. Phys. **126**, 184507 (2007)
4. J.-J. Max, C. Chapados, J. Chem. Phys. **126**, 154511 (2007)
5. J.-J. Max, C. Chapados, J. Chem. Phys. **127**, 114509 (2007)
6. J.-J. Max, C. Ménichelli, C. Chapados, J. Phys. Chem. A **104**, 2845 (2000)
7. J. Baril, J.-J. Max, C. Chapados, Can. J. Chem. **78**, 490 (2000)
8. J.-J. Max, C. Chapados, Appl. Spectrosc. **53**, 1045 (1999)
9. J.E. Bertie, H.H. Eysel, Appl. Spectrosc. **39**, 392 (1985)
10. J.E. Bertie, M.K. Ahmed, H.H. Eysel, J. Phys. Chem. **93**, 2210 (1989)
11. J.E. Bertie, Z. Lan, Appl. Spectrosc. **50**, 1047 (1996)
12. T. Hirschfeld, A.W. Mantz, Appl. Spectrosc. **30**, 552 (1976)
13. D.J. Moffat, D.G. Cameron, Appl. Spectrosc. **37**, 566 (1983)
14. M.F. Faggin, M.A. Hines, Rev. Sc. Instr. **75**, 4547 (2004)
15. P.J. Farrington, D.J.T. Hill, J.H. O'Donnell, P.J. Pomery, Appl. Spectrosc. **44**, 901 (1990)
16. H.M. Heise, Appl. Spectrosc. **41**, 88 (1987)
17. J.-J. Max, C. Chapados, Appl. Spectrosc. **62**, 1167 (2008)
18. A. Kucirkova, K. Navratil, Scripta Fac. Aci. Nat. Univ. Masaryk. Brun. **23**, 5 (1993)
19. F.R.S. Clark, D.J. Moffatt, Appl. Spectrosc. **32**, 547 (1978)
20. A.M.A. Pistorius, W.J. DeGrip, Vibr. Spectrosc. **36**, 89 (2004)
21. T. Iwata, J. Koshoubu, Appl. Spectrosc. **48**, 1453 (1994)
22. H.R. Zelsmann, J. Mol. Struct. **350**, 95 (1995)
23. D.A. Wieliczka, S. Weng, M.R. Querry, App. Opt. **28**, 1714 (1989)
24. T. Fujiyama, J. Herrin, B.L. Crawford Jr., Appl. Spectrosc. **24**, 9 (1968)
25. J.K. Vij, Int. J. IR MM Waves **10**, 847 (1989)
26. H.J.K. Köser, Fresenius Z. Anal. Chem. **317**, 845 (1984)
27. G. Dutier, A. Yarovitski, S. Saltiel, A. Papoyan, D. Sarkisyan, D. Bloch, M. Ducloy, Europhys. Lett. **63**, 35 (2003)
28. H. Fröhlich, *Theory of Dielectrics: Dielectric Constant and Dielectric Loss*, 2nd edn. (The Clarendon Press, Oxford, 1958)
29. N.A. Marley, J.S. Gaffney, M.M. Cunningham, Appl. Opt. **33**, 8041 (1994)
30. L. Kou, D. Labrie, P. Chylek, Appl. Opt. **32**, 3531 (1993)
31. S.Y. Venyaminov, F.G. Pendergast, Anal. Biochem. **248**, 234 (1997)
32. G.R. Fowles, *Introduction to Modern Optics*, 2nd edn. (Dover Publications, New York, 1989)
33. J.P. Hawraneck, P. Nerlakantan, R.P. Young, R.N. Jones, Spectrochim. Acta **32**, 75 (1976)
34. W.H. Wolfe, G.J. Zissis (eds.), *The Infrared Handbook* (Office of Naval Research, Washington, 1978)
35. W.G. Driscoll, W. Vaughan (eds.), *Handbook of Optics* (McGraw Hill Book Co, New York, 1978)
36. J. Max, *Méthodes et Techniques de Traitement du Signal et Applications Aux Mesures Physiques, Tome 1*, 4th edn. (Masson, Paris, 1985)
37. B. Czarnik-Matusewicz, S. Pilorz, J.P. Hawranek, Anal. Chim. Acta **544**, 15 (2005)